Research Square

Preprints are preliminary reports that have not undergone peer review.
They should not be considered conclusive, used to inform clinical practice,
or referenced by the media as validated information.

Geo-Environmental Monitoring and 3D Finite Elements Stability Analysis for site Investigation of Horemheb Tomb (Kv57), Luxor, Egypt

Sayed Hemeda (sayed.hemeda@cu.edu.eg)
Cairo University

Research

Keywords: Geo-environmental investigation, Remote sensing, GIS, 3D Geotechnical Modeling, Thebes Formations, Esna shale, rock support structure, Horemheb tomb (KV57), Valley of the Kings, Rock cut tomb

Posted Date: August 7th, 2020

DOI: https://doi.org/10.21203/rs.3.rs-45712/v1

License: This work is licensed under a Creative Commons Attribution 4.0 International License.
Read Full License

GEO-ENVIRONMENTAL MONITORING AND 3D FINITE ELEMENTS STABILITY ANALYSIS FOR SITE INVESTIGATION OF HOREMHEB TOMB (KV57), LUXOR, EGYPT.

Sayed Hemeda

Professor, Conservation Department, Faculty of Archaeology, Cairo University, Egypt.

Fax: 0235728108. P.C 12613. email: sayed.hemeda@cu.edu.eg

ORCID ID: https://orcid.org/0000-0003-0308-9285

Abstract:

The Valley of the Kings (KV) is a UNESCO world heritage site with more than thirty opened tombs. Recently, most of these tombs have been damaged and inundated after 1994 flood. The Pharaonic rock-cut tombs at the valley of kings at the west bank of Luxor, were excavated mainly in the lower member I of the Thebes Limestone Formations and Esna shale Formations. These underground structures show serve degrees of damage and disintegration of supporting rock pillars, sidewalls and ceilings. In order to understand the Geo-environmental impact mainly the past flash floods in particularly the 1994 flood due to the intensive rainfall storm on the valley of kings and the long-term rock mass behavior under geostatic stresses in selected Horemheb tomb (KV57) and its impact on past failures and current stability, Remote sensing, GIS, LIDAR, 3D finite element stability analysis and rock mass quality assessments had been carried out using advanced methods and codes.

Geo-environmental monitoring and numerical analysis play an important role in the tunneling and underground works, especially for archaeological underground structures are subjected to large initial stresses and high overburden geostatic stresses. These conditions yield non-reversible deviatoric shear and creep strains that develop during time at constant stress and eventually increasing the rate of strain, namely the secondary and tertiary creep stages. Neglecting time effects may lead to incorrect evaluation of deformation, which may impact the criteria for selection of proper design. In order to describe the deformation in underground structures in the valley of kings, various approaches have been established based on analytical, empirical and numerical methods. It is clear that the tomb of Horemheb (KV57) is much more susceptible to surcharge geostatic loading from the overburden rock strata, rock bursting, and structural damage of support pillars and walls induced to the water and past/recent flash floods impacts caused by heavy rain in the Valley. Since some of this tomb also makes contact with the underlying shale layers, that have high activity and the potential for swelling and shrinkage under changing moisture conditions.

Our work provides environmental satellite space views via landviewer EOS Platform with passive and active sensors which includes the NDVI, SAVI, ARVI, GCI, NBR, NDSI, LIDAR images, Terrain DEM Digital Elevation Models, 3D geological maps. In other hand experimental and Numerical geotechnical evaluations and modeling of the rock mass of these underground structures and their surroundings have been executed. We estimated the rock mass quality of the different members within the Thebes limestone and Esna shale formations using the mechanical testing and Rock Mass Rating (RMR), rock quality system (Q-system) and Geological Strength Index (GSI) systems.

Our analyses show that the KV57 rock- cut tomb at Luxor has been cut into poor to very poor quality marl shale masses. Rock failures of ceilings and pillars were frequently facilitated by local, unfavorably oriented persistent discontinuities, such as tension cracks and faults. Other failures were related to the disintegration of the marl limestone and Esna shale Formations into individual nodules upon weathering. Our data suggest that, in ancient Egypt monumental tomb construction, low-strength rock masses rarely resulted in modifications of the planned tomb design in order to minimise the risk of rock falls and to prevent collapses. The current flood protection measures are not enough. For this two following measures are proposed 1- to rise the current wall by 50cm. 2- to fill the depression by reshaping bathymetry.

Key words: Geo-environmental investigation, Remote sensing, GIS, 3D Geotechnical Modeling, Thebes Formations, Esna shale, rock support structure, Horemheb tomb (KV57), Valley of the Kings, Rock cut tomb.

1. Introduction:

Previous years UNESCO reports indicated, among other things, the following factors, which were considered to have a severe impact on cultural heritage properties:

- Flood hazards (valleys of kings and queens).

- High groundwater level

- Lack of a comprehensive management plan

- Major and ongoing infrastructure and development projects

- Uncontrolled urban development

- Residential and agricultural crawl or creep on the west bank of the Nile.

Great efforts have been made to preserve the archaeological site of the Valley of the Kings (KV) since UNESCO declared it a World Heritage Area in 1979. Explorations have been made to restore monuments and temples and investigate damage, degradation, and risk structures by many international groups of scientists inside and around KV (For example, Theban Mapping Project 2019, Dragowski 1988, Rutherford 1990, Verdel 1993, Lazar 1995, Wüst 1995, Fitzner et al. 2002, Hamada et al. 2004, Tawfik et al. 2010, Dupuis et al. 2011, Cuezva et al. 2016, Bardají et al. 2017, Ziegler and others. 2019). Piguet et al. 1988, Olivares et al. 2019, Hemeda. 2018 summarize that Egyptian monuments mainly fail due to deterioration or cracking of building materials, weak soft soil (for example, clay), and displacement along natural fractures in hard rocks (for example, limestone, sandstone, strong clay), Or falling rock from steep slopes drifts.

The Valley of the Kings was a burial place for Egypt's pharaohs during the reign of the new king from 1550 to 1070 BC. KV is a small valley cut by heavy rain and eroded during several periods of rivers in the Eocene into a thick layer of limestone located around a sliced layer of marly shale. The valley is located at an altitude of 70 meters above the level of the Nile River (140 meters above average sea level) and the height of the surrounding hills is 80 meters above the valley floor, as shown in Figure 1. During the late eighteenth dynasty and throughout the nineteenth century, royal tombs were usually located below the valley some distance from the rock walls. Builders often take advantage of their ankle

slopes, as in the case of the Horemheb KV57 tomb. Indeed, many other royal tombs in the Valley of the Kings exhibited similar decay and disintegration features. Most of the royal tombs in the Valley of the Kings and the Western Valley were excavated in the limestone of the middle and lower part of the first Thebes' member, the lowest unit of the formation of Thebes. However, many tombs penetrate the rock and interlocking rocks found in the formation of Isna Shale. All show a advanced deterioration in the rock structure that is irreversible due to swelling and contraction. The Horemheb tomb KV57 is clearly more susceptible to the additional geostatic loading of overburden or surcharge heavy rock layers, rock bursts, and structural damage to support pillars and sidewalls and the effects of past / recent rapid floods caused by torrential rains in the valley. Since some of these tombs also come into contact with underlying shale layers, which have the potential to swell and shrink in conditions of variable humidity. Extensive damage to these underground structures was widely observed in the Valley of the Kings. This tomb KV57 tends to be the worst tomb preserved in the Valley of the Kings. The marl shale in the valley is particularly weak and unstable. Not only did the old quarry problem come up, but the modern conservators too. When the marl shale comes in contact with moisture, it expands and can literally rip the hillside. Despite being thin, being strong support elements, these shafts will continue to attract significant loads due to redistribution of stress due to drilling. Insufficient column strength can lead to extreme instability and failure of the adjacent rock mass with potential catastrophic consequences for the associated undergrounds.

Today, satellite imagery like Guardian 2 is systematically available free of charge for large coverage, and can be used for accurate mapping as well as for documenting and analyzing historical and contemporary human activities around cultural heritage sites.

The paper represents the first comprehensive empirical and numerical studies to analyze the engineering failure and the appropriate design of the permanent mechanical support system for the Tomb of Horemheb (KV57). It is in fact one of the largest rock tombs found in Egypt.

The main characteristics of the geo-environmental and geotechnical analyzes conducted in this study are the investigation of the stable stability, safety margins, and engineering failure of the Tomb of Horemheb (KV57) under their current conditions, against the unfavorable environment (i.e. widespread weathering due to the impact of water and sudden floods in the past and present in particular the 1994 flash flood), Complete lack of protection, geostatic overload of structural rock support columns, and severe geotechnical and seismic conditions. Also to design a suitable geotechnical support system, according to the engineering rock block rating, in particular the RMR rock block rating and the Q-system index of high-quality rock tunnel.

Engineering analysis was carried out through the following four main steps: 1- Evaluation of surrounding rocks (marl limestone and marl shale) by experimental research and Roclab program to obtain the Hoek Brown and Mohr- Coulomb fit classification criterion and rock mass standards in particular the global strength and deformation coefficient. Also to specify the maincharacteristics of the Esna Shale using different methods such as swelling test, swelling potential, swelling pressure, in addition, discussion of the role of the

expansive Esna Shale in the deterioration of archaeological buildings and sites. 2- Quantitative and qualitative estimates of the relevant factors affecting the stability of the tomb, especially overloading, fixed, geographic, and dynamic. 3- Integrated 3D geotechnical modeling of the cemetery environment for stress and displacement analysis and identification of volumetric strains and plastic points using advanced symbols and programs such as PLAXIS 3D. 4- The rapeutic and retrofit policies and techniques and the fixed monitoring and control systems needed to strengthen and stabilize the cemetery, where the rock mass classification refers to the rock mass where KV57 is excavated and it is poor rocks. The mechanical behavior of the rocks is simulated by assuming a foundational model to soften the elastic stress of the flexible plastic that captures fragile failure and the mechanisms of progressive substrate failure. In addition, rock pillar treatments and ground support strategies are discussed.

Based on the theory of stable engineering equilibrium and rock mass classification, support structure techniques are provided and detailed in detail with the KV57 case in this study.

2. Aspects of the strengthening design of the underground monuments.

Strengthening design of underground monuments the following aspects are to be considered:

- Type and purpose of the underground structures

- Alignment

- Site Investigation

- Topographical conditions

- Geological and hydrological conditions

- Environmental impact including, noise, vibrations and air pollution

- Legal aspect

- Safety requirements

- E& M requirements

- Geotechnical prognosis and identification of typical ground characteristics and definition of ground properties (key parameters) for analysis

- Risk assessment and analysis (Geotechnical Monitoring)

Geotechnical monitoring includes Typical 3D displacement measurement in the underground excavation and on the surface (if required), extensometers, sliding micrometers, inclinometers, transducers, electrical stain gauge, load cells for rock bolts, pressure cells, and piezometers are used to observe the system behavior. To enable a quick visualization, reliable evaluation and interpretation of monitoring results, special software like PLAXIS 3D is required.

- Selection of Support methods

- Integration of operational systems to address the underground excavation safety requirements (ventilation, firefighting).

3. Historic Context and Architectural design

This is the most innovative realization that Horemheb left in Thebes.The tomb itself is located inside the western branch of the southwest wadi. The opening of the tomb is cut low into the hill and once inside the tomb, the way further inward is by a set of stairs cut out of the rock. His plan is coupled with a change in axis, as at the beginning of the dynasty, with the straight outline of Amarna's tombs. It measures approximately 110 m. The length of the sarcophagus is about 30 meters. Below is entry. Approaching north from the stairs entering the burial chamber, the only deviation is in the pillar hall just behind the well chamber. Here the stairs leading to the lower levels are compensated to the west (opposite the Western Wall), but progress is almost parallel to the stairs and upper aisles.

The burial chamber consists of two levels, the first, the upper level, which is a hexagonal hall. This leads to the lowest level, which is the actual resting place of the sarcophagus. Of these two sections there are a total of nine appendices, the furthest (most northerly) only partially drilled. The tomb was penetrated in ancient times. Besides digging pits through the upper passages and stairs leading to the well chamber, thieves also penetrated the far wall of this chamber, to reach the bottom of the grave. The thieves clearly do not get fooled by the clogged, deadly back wall.

Upon its discovery, by Davis, the tomb was found to still contain many items of interest. These included a red granite sarcophagus and a calcite chest calcite. There were also many wooden figures of the deities, as well as the king-size wooden statues of the king, reminiscent of those in the tomb of Tutankhamun, but without gilding. The diggers in the room, known as the Osiris Chamber, discovered the bones of two women and in the

sarcophagus, the bones of two women and another man. In the coffin remains were found, which Davis was unable to identify, belonging to a man or woman. The mummy of Horemheb has not been found and has not yet been identified.

The decoration inside this tomb was organized as follows: (Figure 2) Entrance corridors and stairs (A-D): not decorated. Well room (E): scenes with the gods. Hall of the upper columns (F): undecorated. Corridor and Ladders (G-H): undecorated. Waiting room (I): scenes with the gods. Entering the burial chamber: the goddess Maat.

Burial Chamber - Pillar Hall (J1): Book of Gates. Burial Chamber - Coffin Room (J1): Book of Gates. Western accessories (K-N): M ("Osiris Chamber") partially, not decorated. Northern appendices (O-Q): undecorated. Oriental Attachments (R-S): undecorated.

4. State of Preservation

Monuments excavated in weak rock and high overburden exhibits fracturing and large deformations due to high stresses around the opening which exceed the ground strength.

The Geotechnical instability problems and degradation phenomena of rock cut tomb of Horemheb (57) in the Valley of the Kings (KV) is likely to be dominated by gravity fall and sliding on structural features, also other factors such as excessively high rock in-situ stresses, creep effect, poor petro-physical and geo-mechanical properties of marly shale structures, weathering and /or swelling rock and flash floods caused by heavy rains in the Valley, vibrations and dynamic loading as well as utter lack of preservation become important and can be evaluated by means of a classification of rock quality. The Esna

shale in the valley is particularly weak and unstable. It not only posed problems to the ancient quarryman, but to the modern conservator as well. When the shale comes into contact with moisture, it expands and can literally tear a hill side apart.

The tomb was robbed in antiquity. Since then, it has been hit by at least eleven flash floods caused by heavy rains in the Valley. These have completely filled the tomb with debris and seriously damaged its comprehensively decorated walls and pillars. In October and November of 1994, two flood events occurred in the Valley of Kings, sending a warning to all heritage managers. In both cases, a local desert rainstorm occurred in the vicinity of the Valley of Kings. Storm-water runoff and sediment entered the Horemheb tomb (KV57) and other many o tombs and caused erosion of gully floors, Table (1) summarizes the he information about 1994 flood and the inundation situation inside the effected KV tombs.

Short-term effects of rainstorms on Horemheb tomb (57) included damaged wall art due to debris flows and collapsed wall structures due to water saturation. Long term damages, however, are difficult to record, even though, their impact might be more critical. Flooded tombs like KV57 built into the Esna shale Formations, are most susceptible to rock-structure deformations or deterioration due to the physical properties of the Esna shale. Throughout the Theban Necropolis, deterioration due to swelling is a common phenomenon that can be observed in Horemheb (KV57).

The damage in KV57 due to the geostatic stresses, consists of fallen ceiling slabs, a cutout wall and door decorations, the ceiling is extremely fractured, however, crack monitors show few displacements since 1991. Crack monitors show a few millimeter (0-

10mm) horizontal and to a more extent, vertical movements. Some parts of ceiling and walls show heavy deterioration caused by rock instability due to abundant horizontal and vertical cracks.

Figure (3) represents the entrance and the main corridor of the Hormoheb tom KV57 where it is whole excavated in the marl Shale layers, Chert lenses and nodules are abundant and obvious. The In-plane deformation patterns like vertical cracks and crown zone rock falling and intensive cracking of lintel due to over loading (geostatic loading) and impact of old and modern flash floods in particular the 1994 flood, as shown in figure (4). Extensive structural damage of crown ceiling zones and engineering failure of the structural pillars, sidewalls and Ceiling of the Corridors and Chambers in the KV57. Brittle rock, high stress conditions lead to rockbursting (the sudden release of stored strain energy) bursts manifest themselves through sudden. Extensive rock falls from the ceiling is obvious and cracks are active, as shown in figure (5). Carved and decorated walls in massive Esna shale Member are in advanced state of disintegration. Showing chert lenses. The ornamented plaster on top of the chert lenses and nodules was damaged during the first flash floods that entered the tomb some 3000 years ago. During several restoration projects over the past 200 years, cracks were filled with plaster for protection and stabilization of the tomb. The impact of the 1994 flash floods on the mural paintings inside the tomb are severely obvious, as shown in figure (6).

5. Materials and Methodology

Remote sensing and GIS

Earth Observation System (EOS) platform is an advanced cloud platform has been used for the search, analysis, storing and visualization of geospatial data. This digital online Platform provided efficient tools for searching, processing, and analyzing large amounts of satellite data which have been created. As a result, valuable insights allowed us to quickly respond to changes in our area of interest (KV).

ELiT (EOS LiDAR Tool) is a sophisticated product based on the complicated algorithms for urban environment modeling and analysis. It provided the original multi-functional approach to LiDAR data processing of the Valley of Kings.

(DEM), Digital Elevation Model Generation – as a representation of the bare earth terrain with uniformly spaced z-values. The DEM tool allowed us to build a Digital Elevation Model that represents the bare earth terrain of the Valley of Kings (KV). This topographic surface is exclusively based on Airborne LiDAR Point Cloud and can be obtained in a form of either DSM (Digital Surface Model) that includes buildings, woody vegetation cover, and other objects or DTM (Digital Terrain Model) with all natural and man-made objects above the ground being removed. Topographical data used in this study is the Digital Elevation Model each cell of which consist of information of X- and Y- coordinates and evaluation Z.

Geotechnical Experimental and Numerical analyses

On other hand, many collected marl limestone and Esna shale samples, where the Horemheb tomb (KV57) is excavated had been investigated by geological and geotechnical investigations, which include XRD, XRF and DTA-TGA analysis and thin section examination under polarized light microscope. A comprehensive program for petro

physical and mechanical testing include the uniaxial compression test and ultra-sonic wave velocity through the materials (PUNDT) has been established. The RocLab program has been utilized to calculate the Hoek-Brown Classification and criterion also to calculate the Mohr- Coulomb fits and rock strength parameters in particularly the deformation modulus. Underground structures of KV57 safety analysis is performed using the finite element (FE) method. The research presents a comprehensive study for the rock cut tombs safety analysis. The safety analysis includes not only a failure analysis but the effect of weathering, in particular the materials wear on the differential settlement have been investigated. The commercial FE package PLAXIS 3D is used for conducting stress, as well as settlement analysis. PLAXIS 3D is a finite element program developed for numerical analysis of geotechnical and underground and subterranean structures.

The deformation of this underground structure has been computed as realistically as possible, utilizing an advanced nonlinear elasto-plastic material model needs to be utilized in PLAXIS 3D which is capable of utilizing such advanced material models. 3D Plastic model is used for deformation and consolidation analysis in this research. The consolidation analysis is performed using PLAXIS 3D. Also in this research.

The Rock Mass Classification calculations are utilized for the general assessment of the rock mass where the KV57 is excavated. The results of the rock mas rating (RMR) and Q-system values were utilized to design an appropriate support system.

6. GEO-Environmental Monitoring and Assessment

Environmental monitoring and assessment discusses developments and technical data arising from environmental monitoring and assessment, principles in designing monitoring systems, and the use of monitoring data in assessing the consequences of natural resource management and pollution risks.

The recent improvements in Earth observation technologies offer advanced technical features that allow new applications especially for documentation, promotion, risk control and preservation of cultural heritage. In particular, the latest spaceflight such as Sentinel-2, Landsate8 OLI + TIRS, Landsate7 ETM + Landsate 4-5 MSS and other satellites are particularly concerned with risk assessment and management, which is obtained systematically for the entire world.

This study provides the possibility of using these modern technological tools in terms of designing and planning smart and sustainable use of cultural heritage resources. The survey showed that most of the environmental problems around the Valley of the Kings come from previous heavy floods due to rainstorms, a high level of groundwater depth and the main cause is unplanned urban encroachment. The results of our analysis showed that the Valley of the Kings is located in the Western Desert with fewer rains and frequencies in the Nile River basin in Egypt. Previous research indicates that the duration of the storm exceeds one to two hours. Most of the storms are low-intensity rainfall since 1994. However, severe rainstorms have been observed in recent years due to the impact of climate change. Currently there is a possibility that a severe storm like one or more intense from the year 1994 may come which could lead to catastrophic consequences especially in these tourist areas. Previous research indicates that the intensity of precipitation in a 1994 storm was about 16 mm / hour within two hours.

The results of our analysis using the data obtained showed the spatial dimension of the changes in urban and agricultural areas, which were clearly shown in the classification images and the extracted indicators. Management and sustainable exploitation as well as conservation and mitigation strategies are mandatory to reduce decay phenomena, threats, and human actions that may accelerate decay dynamics or lead to degradation and / or significant change in rock graves in the KV and its "environment". In this context, remote sensing technologies can provide useful data to update information and documents in a timely manner as well as reliable tools for systematically monitoring cultural property. The tremendous availability of advanced remote sensing data today has opened up unexpected new and future challenges for several years. In particular, for archaeological sites and remote sensing of landscapes, it can provide useful data not only for exploring the surface of the Earth to detect sites and artifacts, but also for management, valuation and conservation, to discover changes as well as to assess degradation and emerging threats.

Figure (7) represents an Urban Image. This band combination also provides a "natural-like" rendition while also penetrating atmospheric particles, smoke and haze. Vegetation appears in shades of dark and light green during the growing season, urban features are white, gray, cyan or purple, sands, soils and minerals appear in a variety of colors. The almost complete absorption of Mid-IR bands in water provides well defined and highlighted sources of water within the image; water is black or dark blue. Hot surfaces such as forest fires saturate the Mid-IR bands and appear in shades of red or yellow. One particular application for this combination is monitoring fires. Flooded areas should look very dark blue or black. Figure (8) represents a band combination which is good for picking out land

from water. In this false color image, land appears in shades of orange and green, and water appears in shades of blue. Figure (9) represents an Index stack; It becomes readily apparent in this image stack that particular colors can be equated to different landscape features. For example, vegetation displays here as green, water as purple, and soil, rocks, and barren land as blue. Clouds also appear as a mixture of purple and magenta, so in this case these indices alone are not sufficient for differentiating clouds from water. Figure (10) represents The classification map which includes four different classes for clouds (including cirrus) and six different classifications for shadows, cloud shadows, vegetation, soils/deserts, water and snow provision of associated quality indicators corresponding to a map of cloud probability and a map of snow probability.

7. The Geology of Gebel El-Gurnah, Luxor

The Thebes Mountains were deposited in a deep, shallow marine environment. The lowest Paleolithic to the early Eocene periods in Western Thebes consist of three configurations: Tarawan, Isna, and Thebes members. The characteristic weathering was used to form a goodness to divide the goodness formation into four units, the first member to the fourth member. The displacement of 30 m of member I associated with the fault of the Valley of the Kings is located on the right side approximately 40 meters from the tomb of Amenemis (KV10), and these formations were deposited in the southern part of Tethys, and the sea connecting the Atlantic and Indian Oceans, which was closed during the continental collision Between the Alps and Africa. Figure 12 represents the digital elevation model of the Valley of the Kings and Mount Gourna. Figure (13) class

succession in the West Bank. Here we show the location of the tombs chosen in this caliphate. The tombs of KV17, 20, TT353 and 192 are located in sub-horizontal rocks. P, Pallucene. E, Eocene.

Jabal Al-Qurna is located about 4 km west of the Nile, opposite Luxor. The main exposed rock units of Jabal Al-Qurna are the limestone formations of Esna Shayl and Taibah. The tombs of the kings were excavated in Thebes formations on the northern side of Jabal Qurna and the tombs of the queens were excavated on the southern side (Dunn, 2014., Wust and Macline 2000).

The main exposed rocks of Jabal Qurna are Esna Shale (Late Paleocene era - early Eocene) and the equally compatible composition of Tiba (early Eocene).

Esna shale: the bottom of 25 m of this formation is less calcareous, usually dark gray-green, and sometimes roughly. The upper rock is grayish-green and green, more compact and holds more gypsum. Iron oxides differ in color. There are red, yellow, brown, and lemon limestones. Gypsum slides run parallel to bed planes. (Wust and Maclane, 2000), as shown in Figure 14. This represents the sudden connection of the Abu Hadd member in the rock formation of Esna with the stone unit 1 of the limestone formation in Thebes. The photo was taken just above the KV57 site.

Esna shale Formation is divided into four distinct lithological units from top to base (Dupuis et al., 2011): 1) Abu Had (alternation of marl and limestone beds with a few clayey intervals. It is lighter in color and richer in carbonate than the underlying member).2) Mahmiya member (dark clayey shale).3) Dababiya Quarry member (dark grey shale from 0.6 to 3.7 m thick).4) Hanady member (light grey massive shale).

The formation of Thebes: The formation of Thebes in the Valley of the Kings can be divided into three members (from the base to the top), the members of Hamada, Baida and Lime. However, the formation of Thebes is above the rock. The bottom part of Hamadat is made of white and chalky limestone with concrete stone, the middle member Beida is made of thick lumpy lumpy limestone, with flint ranges extending parallel to the bedding planes, the upper member Al-Geer is mainly made of white limestone, (Aubry et al, 2008 and Silotti, 1997).

There are many faults in the SW corner of the Valley of the Kings. It is very complex in nature. The number of faults cuts Eocene limestone formations. Usually, these separators bring about varying cross-slipping problems, and veins have developed around crystalline calcite in the overlapping spaces. Calcite may be strict in addition to structures that go beyond packages, which provide the course with more rationality than demanding a coupon.

Regular defects, which illustrate the level evolution of the NE-SW trend, are abundant. However, one major mistake, on the northwestern side of the valley, may be the dominant slip (and left left), while others need oblique help (left-normal, regular right rotation). Although these five measured errors are not sufficient, it will be an opportunity to be statistically significant. Where fragile rocks lead, high pressure conditions cause the rocks to burst (the sudden release of stored stress energy) manifested by sudden.

Figure (15) is an indication of the corrosion caused by the rapid flooding of marl shale and vertical cracks in Unit 1 of the limestone in Thebes, and the identification of abandoned excavations and its bridge. The sub-vertical wall pieces were drilled at the top of the shale

formation and at the base of the limestone formation in Thebes. The white arrows indicate the grooves of erosion in the lower part of Unit 1 of the formation of Thebes, in the Hanadi member (Isna rock formation) and in the debris covering the Isna composition. Note that the grooves at the base of the limestone in Thebes and slightly lower are generally cavity, especially at the top and bottom of the protruding base of Unit 1. These are potential signs of sudden flooding. Falling blocks are unstable vertical mass and open vertical fractures; degrees. The dunes resulting from archaeological excavations.

8. Results of the experimental investigation:

8.1 Mineralogical and Geotechnical properties of intact marl limestone and marly Shale specimens and discontinuities

The tomb was cut into a south-facing flank of the lowermost unit of the Thebes Formation.

The tomb is built into Esna shale Formation, 152.59m asl.

Eight thin sections were examined using a polarized optical microscope to determine the petrographic and geochemical properties of these building materials (Marl limestone and marly Shale). X-ray diffraction sensors (XRD) and X-ray probe (XRF) were performed to determine slats and proportions of the fixing limestone and Shale. In addition to the electron microscopy (SEM) attached to the energy dispersed x-ray (EDX) for microscopy and microscopy. Examples of XRD diffraction are increased for both studied stones and slurry tests by Cu K. radiation. The filtering speed is 2θ = 1 ° / min. With a constant voltage of 40 kV, 30 m and using X-ray diffraction PW 1480. Important components (by weight%)

of the studied stone and rock tests were performed using X-ray fluorescence spectroscopy (XRF) along an advanced wavelength - dispersive spectroscopy (Axios, WD-spectroscopy) XRF, PANalytical, 2005, Netherlands). Chemical analyzes were performed using the ASTM specification (ASTM C114-00, (ASTM C114-15))), and electron microscopy images (SEM) were performed on a smaller analyzer JXA 840A for electron testing, Japan,

The engineering properties of the studied building materials were achieved. 13 cylindrical samples of limestone and marly Shale were prepared to determine the petrophysical and geochemical properties. Specific gravity (G_S), Bulk unit weight (γ_b), water absorption (W_c), porosity (n) and saturation (Sr) are the specified physical aspects. While mechanical characterization involved determining the uniaxial compression force (σ_c), Young (E) coefficient and discrete Brazilian tensile strength (σt), shear cut (T), and Schmidt hammer index (SHV) number, strength or impact indicators are estimated By AIV, in addition to testing non-destructive ultrasound velocity (Vp) by stone examples, Young's dynamic coefficient (Edy) and shear modulus (G).

Mineralogical study

The upper Esna Shale II unit is composed of marl and shale interbeds. The marl interbeds of Esna Shale II and the marls of Member I have similar compositions. The marls of Esna Shale II have 65–70%calcite and 30–35%clay minerals.

The clay minerals are mainly palygorskite (50– 80%), kaolinite (10%) and illite/smectite mixed layers (10–40%). The mineralogical composition of the shales is 5–25%calcite, 5–

10%anhydrite and 70–80%clay minerals. The clay minerals are predominately illite/smectite mixed layers (40– 75%), palygorskite (20–50%), kaolinite (<10%) and illite (<10%). The lower unit of the Esna Formation, Esna Shale I, has up to 20%calcite and up to 95%phyllosilicates, with 3–10%anhydrite. The clay minerals are composed of about 70%kaolinite, 25–35%illite/smectite mixed layers and minor amounts of palygorskite and illite, as shown in figure (16).

In the four samples analyzed, calcite (marl) and clay minerals (shale) are most abundant with minor amounts of quartz. The detected clay minerals are mixed-layer smectite, palygorskite and sepiolite. The clay minerals account for up to 80% of the mineral composition in the shales.

Small amounts of quartz, abundant palygorskite and little sepiolite were detected in the marl of the lowermost part of Member I. The clay mineral composition is 10%sepiolite and 90% palygorskite.

The XRD analysis indicated that the major contents of Esna shale are quartz (SiO_2) and Montmorillonite ($Na_{0.2}$ $Ca_{0.1}$ Al_2 Si_4O_{10} $(OH)_2$. (H_2O) $_{10}$, the minor contents include the Kaolinite and Illite with Calcite traces, as shown in tables (2 and 3). The X- ray Diffraction results showing the clay minerals of natural or air treated untreated clay fractions sample from Esna shale Member, where the Horemheb tomb (KV57) is excavated are Montorillonite 77%, Illite 20% and Kaolinite 3%, as shown in Figure (17) and tables (4). Table (5) summarizes the X- ray Diffraction results of three shale samples in the three levels from Esna shale Member at the site of KV57. Figure (18) respresents the XRD for the air dried, ethylene glycol treated, and heated to 550C clay fractions from samples of

Esna shale, showing decrease and disappearance of peak of Illite/Smectite (I/S) and the present of the Montimorillonite.

Thin-sections prepared on the marl limestone and Esna shale samples where the KV57 is excavated. C.N. Microscopic photograph shows the marl sample from Member I is very fine-grained to fine-grained. Considerable amounts of cavities and microvienlets filling by recrystallized dolomite are observed in the micritic calcite matrix. The rock is very to fine-grained and composed mainly of calcite and dolomite as the essential components associated with minor amount of clay minerals and rare amounts of microcrystalline quartz, iron oxides and opaques. Calcite represents the matrix of the rock and occurs as very fine-grained (micrite), anhedral to subhedral interlocked crystals. Dolomite occurs as very fine to fine-grained, euhedral to subhedral crystals and filling microvienlets and cavities. Quartz is detected as very fine-grained crystals scattered in the matrix. Some pores of irregular shapes and various sizes are observed scattered in the rock. Some parts of the sample are stained by iron oxides, as shown in Figure (19). C.N. Microscopic photograph shows the Esna shale sample is very fine to fine-grained (mainly sand size), well sorted that is cemented by minor amounts of iron oxides, clay minerals and carbonates. The sample is porous where pore spaces of different sizes are observed. The rock is composed mainly of quartz and feldspar grains cemented by minor amounts of iron oxides, clay minerals and calcite. Rare amounts of muscovite, biotite, hornblende and opaque minerals are observed in the sample. Quartz occurs as very fine to fine grains of subrounded to angular shape. Feldspars occur as fine grains that are observed in different parts of the sample. Opaque minerals occur as very fine to fine-grained crystals, scattered

in the sample. Some parts of the sample are stained by traces of iron oxides, as shown in figure (20).

Geotechnical study

Marl limestone: Petro-physical properties: Physical measurements referred that the unit weight (γ) of marl limestone of KV57 is between 20 and 21 kN/m^3, water absorptions (*Wa*) were between 10 and 12% and the apparent porosity (*n*) ranged from 14 to 19%.

Shear Wave Velocities (*Vs*): Shear wave velocities of limestone samples were measured by PUNDT (ASTM 597, ASTM D 2845-83). They varied from 0.7 to 0.9 km/s (with an average of 1 km/s for an orientation perpendicular on the bedding plane.

Uniaxial Compression Test**:** The compressive strength (σ_c) for the sidewalls is between 8 and 9 MPa.

The static Young's modulus (*E*) = 12GPa, Poisson Ratio (*v*) = 0.25-0.30, figure …. shows the test set and the results are summarized in table (6).

Esna shale: The physical properties includes, The bulk unit weight of the Esna shale is 1.79 to 1.86 g/cm^3, and the uniaxial compressive strength is 4.22 to 4.43 kg/ cm^2, the specific gravity GS = 2.7, the void ratio e_i =1.86, γd =17-18 N/m^3, γb = 18-20 N/m^3, water content 8-10%, OMC 14-16%, LL 75-80%, PI 422-432 %, clay % 70-80. The Esna shale

has poor elastic parameters, where the static modulus of Elasticity E =1500- 2000 kN/m^2 and the Poisson's ratio υ = 0.3- 0.4. For the shear strength parameters for this also very poor, where the cohesion of grain particles c = 30 kN/m^2, and the internal friction angle ϕ=25. Free swelling % 100 -180, and swelling pressure 710-742 kPa. The Activity % is 1.5 - 2 . Results are summarized in tables (7).

Long term swelling test on Esna shale samples revealed an enormous water absorption and swelling capacity. Swell heaving is between 50% and 80%. Most of which take place within the first hour. The swelling pressure exceeds 5 MPa and 13 MPa with deformations of 1.5 and 3.3%, respectively. Table (8) summarizes the geotechnical properties of the intact marl limestone samples with depth and the shear parameters of the discontinuities of the rockmass where the Horemheb tomb (KV57) is excavated.

According to the ASTM C568 / C568M-15 the physical characteristics of the marly limestone and marly Shale are low, since the water absorption by weigh/max must be in range of 3% for the low density limestone to 12 % for the high density limestone.

According to the ASTM C 170, C 880, C 99 test methods and ASTM C568 / C568M-15 specifications, the physical and mechanical characteristics of the marly limestone and marly Shale is low, since the standard requirement for the uniaxial compressive strength (σc) of the limestone must be in range of 12 MPa for the low density limestone to 55 MPa for the high density limestone, (Hemeda, 2020).

8.2 Analysis of rock mass strength using RocLab Program

RocLab is a software program for determining rock mass strength parameters, based on the latest version of the generalized Hoek-Brown failure criterion.

Hoek-Brown Classification: Intact uniaxial compressive strength of intact marly limestone (σ_{ci}) = 8 MPa, GSI geological structure index = 50, intact modulus *(mi*) =9, disturbance factor (*D*) = 0, intact rock deformation modulus *Ei*= 12000 MPa, modulus ratio (*MR*) =500.

The generalized Hoek-Brown Criterion failure criterion: *mb*= 1.509, *s*= 0.003866. *a*= 0.50573, where (s) and (a) are constants of the rock mass, calculated from the geological strength index (GSI) and disturbance factor (D).

Mohr-Coulomb Fit: Cohesion *c*= 0.3859 MPa, Friction angle φ= 29.62^{o}

Rock mass parameters: Tensile strength of intact rock σ_t = -0. 016 MPa, Uniaxial compressive strength 800 kPa, as shown in Figures (21) and (22). Table (9) summarizes the Hoek Brown classification, Hoek Brown Criterion, Failure Envelope Range, Mohr-Coulomb Fit and Rock mass parameters for the marl limestone member 1 where the entrance Horemheb tomb (KV57) is excavated, using the RocLab program.

9. Results of the 3D Numerical Analysis and Geotechnical Modeling:

In this study, PLAXIS 3D was implemented to determine the behavior of shale formations under heavy geostatic pressures. Plaxis is a commercially available program that uses the FEM Finite Element method. Plaxis uses various soil / rocks models to determine the soil / rocks behavior such as Mohr-Coulomb model, hardening soil model, soft soil model, soft

soil crawl model, common rock model and modified Cam-Clay model. The hardening soil model was chosen for this study.

The hardening soil Model is an advanced model of soil behavior simulation. For the Mohr-Coulomb model, specific stress states are described by the friction angle phi, the cohesion c and the expansion angle psi. However, soil hardness is described more accurately using three different types of input hardness: E50 three-axis hardness, Eur three-axis dumping hardness and Ooed counter load hardness. Unlike the Mohr-Coulomb model, the hardened soil model also explains the stress dependence of hardness standards. This means that all stiffness increases with pressure. Hence, the hardness of the three inputs relates to the reference pressure, and is usually taken as 100 kPa (1 bar).

Besides the above model parameters, primary soil conditions, such as pre-standardization, play a fundamental role in most soil deformation problems. This can be taken into account in generating the initial pressure.

Low-strength shale formations where KV57 is seriously excavated grave safety under static loading and earthquake conditions. PLAXIS 3D was used for three-dimensional numerical analysis of the central main rooms with their structurally supportive rock columns structurally damaged. Vertical cracks due to overload and slope of strength are evident.

The goal of 3D testing is to evaluate the state of pressure in columns taking into account 3D engineering. The issue of 3D effects on a basic design methodology is considered in the following areas. The various reenactments shown are redirected using the PLAXIS 3D symbol (PLAXIS 3D).

The results of the three-dimensional static analysis represented in Figure. (23) to Figure. (31) Indicate that the rock columns in the main chambers are subject to relatively high pressure pressures. The main effective calculated compression peak pressure for rock columns and supporting side walls is 5.52 x 10^3 kN/m^2 as shown in Figure (23). The maximum effective vertical compressive pressure calculated on rock columns and supporting side walls is 8.7 x 10^3 kN/m^2 as shown in Figure (24). The effective horizontal mean presses 4.94 x 10^3 kN / m^2 as shown in Figure (25). Figure (26) represents the plastic dots (Mohr-Coulomb and Tension cut points) for the roof, the supported rock columns and the sidewalls of KV57. The total displacement of the roof and pillar areas is 30.92 mm as shown in Figure (27). The vertical displacement is 30.76 mm as shown in Figure 28. The horizontal displacement is 15.52 mm as shown in Figure (29). The total incremental displacement is 1.07 mm as shown in Figure (30) and the volumetric strain is 1.45% as shown in Figure (31).

The results showed that the values of stress and displacement distribution on the roofs and structural rock pillars did not increase due to the excavation process extending behind the main hall and this may be due to the lower level of the ceiling for these small burial chambers. Numerical results suggested that failure could be more influenced by the orientation of vertical joint sets rather than bedding planes.

The numerical analysis reveals that the roof of the tomb which has suffered from exfoliation is those in compression. Given that the exfoliation is the result from a combination of the fluctuation of humidity and compressive stresses, the study concludes that the fluctuation of humidity needs to be minimizes by preventing the active circulation of air through the tomb.

Pillars axial stress versus displacement curves provide insightful information on pillar failure mechanism associated with increasing axial loads. It can be seen that for pillars with W/H = 1/3 ≤ 0.5 the pillars generally exhibit a linear elastic behaviour up to peak strength then a brittle failure followed by an approximate perfectly plastic post-peak behaviour.

The results indicate general agreement with the empirical relationship for pillar width to height ratios. On the other hand, there is a significant reduction in pillar strength for ratios W/H<0.5. In these cases and where the pillar stability is controlled by unfavourable defects.

10. Evaluate the safety factor and stress state in the structural support pillars

Factor of Safety = FoS = $\frac{\text{Strength of Material}}{\text{Max Computed Stress}} = \frac{\text{Failure Stress}}{\text{Actual Stress}}$

FoS >1 is The design criteria the engineering component/structure must achieve.

The designer defines failure; component/structure doesn't meet performance criteria;

e.g. excessive deformation, fracture, etc.

In general, Use higher FoS for brittle materials (to avoid catastrophic failure). Use lower FoS when using materials for which the material properties are very well known. Use higher FoS for uncertain environments/stresses.

Typical Values for the Factor of Safety (FoS) of the buildings is ≥ 2. Bolts ≥8.5.

It is demonstrated that induced stresses of significant magnitude and ambiguous distribution are to be expected in the supporting pillars. Multiple openings and excavations designed on the basis of the average stress in the pillar σv^{-} given by the tributary area theory, as explained in equation (1).

$$\sigma v - = \frac{At}{AP}\ \sigma v \qquad (1)$$

Where,

- A_t is the area supported by the pillar
- A_p is the area of the pillar
- σ_v is the vertical stress at the level of the roof of the excavation (catacombs)

To evaluate the degree of safety of a pillar, we must be compare the above average pillar stress $\sigma_v$with the pillar strength σ_p. The latter is not simply the unconfined compressive strength of the material comprising the pillar q_u, because shape and size effects introduce significant modifications from the breaking strength of unconfined compressive cylinders.

The strength in compression for rectangular pillars of square cross section can be estimated from the equation number (2).

$$\sigma_p = \{0.875+0.250\frac{W}{H}\}\ \{\frac{h}{hcri}\}^{0.5}\ (q_u) \qquad (2)$$

Where,

- σ_p is the strength of the pillar,
- W and H are the width and height of the pillar respectively,

- q_u is the UCS strength of the pillar material on cylinders with height (h) equal to twice the diameter and

- h_{crit} is the minimum height of the cubical specimen of pillar material such that an increase in the specimen dimension will produce no further reduction in strength.

For the pillars, see figure (24), σ_v=8.7 MPa, A_t = 2 m^2 and A_p =1 m^2 we can derive:

$$\sigma v^{-} = \frac{2}{1}\, x 8.7 = 17.4 \text{ MPa}$$

The strength of the pillar σ_p can be estimated from the equation: For the pillar we have W=1 m, H=3m. If we assume h_{crit}=0.2 m and h=1 m for q_u = 8 MPa, we have σ_p = 17 MPa

And the Factor of Safety F. S = $\frac{\sigma p}{\sigma v-} = \frac{17}{17.4}$ = **0.97** which very low and indicate to the dangerous and unsafe situation and losing of the structural function of these load bearing pillars. Hoek and Bray quote Salamon and Munro's suggestion of acceptable safety factors > 1.6. Such values may be adequate for the excavation stability, (Hemeda et al, 2010, Hemeda, 2018).

Also overstress state = $\frac{\sigma c}{\sigma v} = \frac{8 \text{ MPa}}{8.7 \text{ MPa}} = 0.9$ (3)

The tributary theory is based on average pillar stresses and derived stress value is generally close to the averages predicted by PLAXIS 3D.On other hand, the overloading of geostatic loading due to the overburden strata on the supporting rock pillars is obvious and it induced critical vertical cracks in these pillars also some sections have an overriding influence on the pillar stability, equation 3, particularly in terms of long-term creep effects and associated strength loss or thinning-out of the effective load bearing pillars and

section, (Hemeda, 2008, Hemeda, 2019). In the original study of Salamon and Munro this occurred between safety factors of 1.3 to 1.9 with the mean being 1.6. This value was recommended for the design of production pillars in South African bord and pillar workings (Salamon and Munro, 1967).

11. Design of structural supporting systems:

In order to effectively manage these large deformations, a number of important strengthening design parameters must be established. These include definition of the over-excavation required to provide deformation allowance, as well as determination of support measures. A support system which allows controlled deformations is chosen to limit the required support resistance and to achieve stability.

The Rock Mass Rating classification system relies on a group of six parameters = Intact rock strength, RQD, joint spacing, joint conditions, groundwater and modulus.

The first option is based on the calculation of Bieniawski, s RMR (Bieniawski, 1989) (rock mass classification system), where the strength of sound rock is 8 MPa (at a rate of 1), the RQD is 50 (at a rate of 12), and the joint spacing is less than 60 mm (5), the interruption conditions are 1-5 mm separation with continuous joints (at a rate of 10) and the groundwater conditions are completely dry (at a rate of 14), to adjust the direction of the joint is -5 and then RMR from the tomb of the sons of Ramses II (37) which are classified as rocks Poor with high pressure, as shown in Table (10).

Pillar Stitching

Pillar stitching with high strength rock bolts provide a significant increase in pillar strength. If a weaker rock layer exists in the pillar, the benefits of pillar stitching were mainly observed as a post-peak behaviour resulting in a more controlled failure, particularly for W/H>0.5.

According to the calculated RMR value and the guidelines for drilling and supporting 10-meter long rock tunnels according to the RMR system (after Bieniawski 1989), as summarized in Table (11), the complete column support system design KV57 can include systematic rockbolt 4-5 meters long, Spaced between 1 and 1.5 m in the crown and walls with a wiremesh 100-150 mm in the crown and inside 100 mm with light to medium ribs of 1.5 m as needed.

Conclusions:

In conclusion, The rock mass properties and environmental conditions of the area were gathered to conduct a preliminary stability assessment the 18 The Dynasty tomb KV57. A 3D numerical model was developed in PLAXIS 3D using the hardening soil modelling method, which indicates the importance of the swelling pressure and vertical joints on the underground structure stability of KV57.

Detailed remote sensing geo-environmental monitoring accompanied with detailed Geotechnical analysis of the Horemheb tomb KV57 in Luxor, Egypt, demonstrated that these unique underground structures offer low static safety factors for roof and structurally

damaged rock pillars under current conditions of geostatic stresses. where the safety factor FS is around 0.97, (note that the acceptable safety factor for underground structures> 1.6 in Static state). The state of the overpressure of the surrounding rocks exceeds the flexible system (field boundaries), and all structural supports of the ceiling, side walls and rock columns are subject to high vertical pressure pressures due to high in-situ stresses and poor geotechnical properties of the marl limestone and marl Shale. Several instability problems of static and dynamic loading have been recorded and analyzed. As a result, a well-focused enhancement and adjustment program is essential and demand urgently since the KV57 is closed due to the instability and unsafe conditions.

Figures Legend

Figure.1. LIDAR image, The Ratio "VV, VH, VV / VH" combination works well for distinguishing water objects, open soils, moistened agricultural fields, vegetation, and urban areas. Water in lakes is shown in dark blue, bright blue or black hues with radar signal noise. Blue hues show agricultural fields with bare soil, often sufficiently waterlogged. Fields with vegetation show a green color. Buildings of a metropolis are represented by bright green-yellow shades.

Figure.2. 3D Sketchup model for the Horemheb tomb, Luxor, Egypt (KV57).

Fig.3. the entrance and corridor of the KV57 where it is whole excavated in the marl Shale layers, Chert lenses and nodules are abundant and obvious.

Fig.4. In-plane deformation patterns like vertical cracks and crown zone rock falling and intensive cracking of lintel due to over loading (geostatic loading) and impact of old and modern flash floods in particular the 1994 flood.

Figure.5. Extensive structural damage of crown ceiling zones and engineering failure of the structural pillars, sidewalls and Ceiling of the Corridors and Chambers in the KV57. Brittle rock, high stress conditions lead to rockbursting (the sudden release of stored strain energy) bursts manifest themselves through sudden. Extensive rock falls from the ceiling is obvious and cracks are active wher the gypsum Pegs are cracked and broken.

Fig. 6. Carved and decorated walls in massive Esna shale Member are in advanced state of disintegration. Showing chert lenses. The ornamented plaster on top of the chert lenses and nodules was damaged during the first flash floods that entered the tomb some 3000 years ago. During several restoration projects over the past 200 years, cracks were filled with plaster for protection and stabilization of the tomb. The impact of the 1994 flash floods on the mural paintings inside the tomb are severely obvious.

Figure.7. Urban Image. This band combination also provides a "natural-like" rendition while also penetrating atmospheric particles, smoke and haze. Vegetation appears in shades of dark and light green during the growing season, urban features are white, gray, cyan or purple, sands, soils and minerals appear in a variety of colors. The almost complete absorption of Mid-IR bands in water provides well defined and highlighted sources of water within the image. water is black or dark blue. Hot surfaces such as forest fires saturate the Mid-IR bands and appear in shades of red or yellow. One particular

application for this combination is monitoring fires. Flooded areas should look very dark blue or black.

Figure.8.This band combination good for picking out land from water. In this false color image, land appears in shades of orange and green, and water appears in shades of blue.

Figure.9. Index stack. It becomes readily apparent in this image stack that particular colors can be equated to different landscape features. For example, vegetation displays here as green, water as purple, and soil, rocks, and barren land as blue. Clouds also appear as a mixture of purple and magenta, so in this case these indices alone are not sufficient for differentiating clouds from water.

Figure.10. The classification map which includes four different classes for clouds (including cirrus) and six different classifications for shadows, cloud shadows, vegetation, soils/deserts, water and snow provision of associated quality indicators corresponding to a map of cloud probability and a map of snow probability.

Figure.11. Location of the Horemoheb tomb (KV57) at the east (main) Valley of the Kings (KV), Luxor Egypt. Stratigraphical succession as seen. Characteristic weathering of the Thebes Formation was used to subdivide the Thebes Formation into four units, Member I to Member IV. A 30 m displacement of Member I associated to the Kings Valley Fault is located on the right-hand side approximately 40 m from the tomb of Amenmesse (KV10).

Figure.12. (DEM), Digital Elevation Model of the valley of kings and the Gebel Gurnah.

Fig. 13. Stratigraphical succession on the West Bank. We show here the location of selected tombs in this succession. Tombs KV17, 20, TT353 and 192 are located in the sub horizontal bedrock. P, Paleocene; E, Eocene.

Fig. 14.Abrupt contact of the Abu Had Member of the Esna Shale Formation with lithological unit 1 of the Thebes Limestone Formation. Photo taken just above the location of the KV57

Fig. 15.Evidence of flash flood related erosion in the Esna Shale and vertical fissures in Unit 1 of the Thebes Limestone, delineation of the abandoned Excavations and its causeway. The subvertical wall-cuts were dug in the upper part of the Esna Shale Formation and at the base of the Thebes Limestone Formation. White arrows point to erosional gullies in the lower part of unit 1 of the Thebes Formation, in the Hanadi Member (Esna Shale Formation) and in the debris that cover the Esna Formation. Note that the gullies at the base of the Thebes Limestone and just below are commonly hollowed out, in particular on top and below the prominent base of Unit 1. These are probable evidence of flash floods. fallen blocks; unstable columnar block and open vertical fissures; screes. screes resulting from archeological excavations.

Figure.16. X- ray Diffraction results showing the bulk Mineralogy of Marl Shale (Calcite/ Smectite) where the Horemheb tomb (KV57) is excavated.

Figure.17. X- ray Diffraction pattern showing the clay minerals of natural or air treated untreated clay fractions sample from Esna shale Member, where the Horemheb tomb (KV57) is excavated.

Figure.18. XRD for the air dried, ethylene glycol treated, and heated to 550C clay fractions from samples of Esna shale, showing decrease and disappearance of peak of Illite/Smectite (I/S) and the present of the Montimorillonite.

Figure. 19.C.N. Microscopic photograph shows The marl sample from Member I is very fine-grained to fine-grained. Considerable amounts of cavities and microvienlets filling by recrystallized dolomite are observed in the micritic calcite matrix. The rock is very to fine-grained and composed mainly of calcite and dolomite as the essential components associated with minor amount of clay minerals and rare amounts of microcrystalline quartz, iron oxides and opaques. Calcite represents the matrix of the rock and occurs as very fine-grained (micrite), anhedral to subhedral interlocked crystals. Dolomite occurs as very fine to fine-grained, euhedral to subhedral crystals and filling microvienlets and cavities. Quartz is detected as very fine-grained crystals scattered in the matrix. Some pores of irregular shapes and various sizes are observed scattered in the rock. Some parts of the sample are stained by iron oxides

Figure. 20.C.N. Microscopic photograph shows the Esna shale sample is very fine to fine-grained (mainly sand size), well sorted that is cemented by minor amounts of iron oxides, clay minerals and carbonates. The sample is porous where pore spaces of different sizes are observed. The rock is composed mainly of quartz and feldspar grains cemented by minor amounts of iron oxides, clay minerals and calcite. Rare amounts of muscovite, biotite, hornblende and opaque minerals are observed in the sample. Quartz occurs as very fine to fine grains of subrounded to angular shape. Feldspars occur as fine grains that are observed in different parts of the sample. Opaque minerals occur as very fine to fine-

grained crystals, scattered in the sample. Some parts of the sample are stained by traces of iron oxides

Figure.21. Major and minor principal stress curve of marl limestone (KV57) using the RocLab program.

Figure. 22. Shear stress-Normal stress curve of Marl limestone (KV57), using the RocLab program.

Figure.23. Effective mean stresses for the supported rock pillars and sidewalls in KV57, the extreme value is 5.52*103kN/m2.

Figure.24. Vertical stresses (sig yy) for the supported rock pillars and sidewalls in KV57, the extreme value is 8.70*103kN/m2.

Figure.25. Horizontal stresses (sig xx) for the supported rock pillars and sidewalls in KV57, the extreme value is 4.94*103kN/m2.

Figure.26. Plastic points (Mohr-Coulomb and Tension cut-off points) for the supported rock pillars and sidewalls in KV57.

Figure. 27. Total displacement (Utot) for the supported rock pillars and sidewalls in KV57, the extreme value is 30.92mm.

Figure.28. Vertical displacement (Uy) for the supported rock pillars and sidewalls in KV57, the extreme value is 30.76mm.

Figure.29. Horizontal displacement (Ux) for the supported rock pillars and sidewalls in KV57, the extreme value is 15.52mm.

Figure.30. Total incremental displacement (dUtot) for the supported rock pillars and sidewalls in KV57.The extreme value 1.07mm.

Figure.31. Volumetric strains for the supported rock pillars and sidewalls in KV57.The extreme value 1.45 %.

Declarations

a. Acknowledgements;

Not applicable

b. Availability of data and materials;

Not applicable

c. Competing interests;

The author declare that he has no competing interests

d. Funding;

The author confirms that he is not currently in receipt of any research funding relating to the research presented in this manuscript.

e. Authors contributions;

The whole database construction and analysis are presented in the manuscript had been achieved by the author. The author read and approved the submitted manuscript.

f. Authors Affiliations;

Sayed Hemeda, Conservation Department, Faculty of Archaeology, Cairo University, Egypt. E-mail address: sayed.hemeda@cu.edu.eg.

g. Availability of Supporting Data;

“Data sharing not applicable to this article as no datasets were generated or analyzed during the current study".

h. Competing Interest;

"Authors have no competing interests to declare"

i. List of Symbols and Abbreviations;

Symbols

At is the area supported by the pillar

Ap is the area of the pillar

σv is the vertical stress at the level of the roof of the excavation (KV5)

σp is the strength of the pillar,

W and **H** are the width and height of the pillar respectively,

qu is the UCS strength of the pillar material on cylinders with height (h) equal to twice the diameter

hcrit is the minimum height of the cubical specimen of pillar material such that an increase in the specimen dimension will produce no further reduction in strength.

β Angle between the normal to the fracture plane and the horizontal plane

ϕ Friction angle of the fracture

x τ Shear stress in resin annulus

σ b Applied stress

α Decay coefficient 1/in which depends on the stiffness of the system

β Reduction coefficient of dilation angle

σ c Uniaxial compressive strength of rock

Aj Joint area

ϕ b basic joint friction angle

Ds Rib spacing

U The shear displacement at each step of loading

c Cohesion between block joints

σ n Normal force

b u Shear displacement

N p Normal force at failure

Qp Shear force at failure

M D Bending moment at yield limit

M p Bending moment at plastic limit

Ei Modulus of elasticity of intact rock

Qcf Shear force

Lcp Reaction length

v Poison ration of rock mass

Po In situ stress

Abbreviations

JRC Joint roughness coefficient

JCS Joint compressive strength

RMR rock mass rating

RQD rock mass Designation

Q rock mass quality

Jn joint set number

Jr joint roughness number

Ja joint alteration number

Jw joint water reduction factor

SRF stress reduction factor

References

Abdallah, T. and Helal, H., (1990). Risk evaluation of rock mass sliding in El-Deir El-Bahary valley, Luxor, Egypt. Bulletin of the International Association of Engineering Géologie-Bulletin de l'Association Internationale de Géologie de l'Ingénieur, 42(1): 3-9.

Alcaíno-Olivares, R., Zeigler, M., Perras, M.A., Maissen, J. (2019). Cliff stability at tomb KV42 in the Valley of the Kings. Egypt: A first approach to numerical modelling and site investigation. . ARMA 19–275

ATHENS, pp. 19-23.

Bardají, T., Martínez-Graña, A., Sánchez-Moral, S., Pethen, H., García-González, D., Cuezva, S., Cañaveras, J.C. and Jiménez-Higueras, A., (2017). Geomorphology of Dra Abu el-Naga (Egypt): The basis of the funerary sacred landscape. Journal of African Earth Sciences. 131: 233-250.

Barton, N.R. (1988) Rock mass classification and tunnel reinforcement selection using the Q-system. In Kirkaldie, L. rock classification system for engineering purposes: ASTM special technical publication 984.1. ASTM International. Pp 59-88

Barton, N.R., Lien R., Lunda, J. (1974) Engineering classification of rock masses for the design of tunnel support. Rock mechanics and rock engineering, Springer. 6(4): 189-236.

Bieniawski, Z.T. (1989) Engineering rock mass classifications. John Wiley and Sons, New York.

Brown E T (2012). Risk assessment and management in underground rock engineering—an overview. *Journal of Rock Mechanics and Geotechnical Engineering*. 2012, 4 (3): 193–204.

Bukovansky M, Richard D P and **Week K R**, (1997) "Influence of Slope Deformations on the Tombs in the Valley of the Kings, Egypt," Proceedings of an International Symposium on Engineering Geology and the Environment, Vol. 3, 1997, pp. 3077-3080.

Cuezva, S., García-Guinea, J., Fernandez-Cortes, A., Benavente, D., Ivars, J., Galán, J.M. and Sanchez-Moral, S., (2016). Composition, uses, provenance and stability of rocks and ancient mortars in a Theban Tomb in Luxor (Egypt). Materials and Structures, 49(3): 941-960.

Deere D U and Varde O A, (1990) "General Report, Engineering Geological Problems Related to Foundations and Excavations in Weak Rocks," Proceedings of the 5th International Association of Engineering Geology Congress, Vol. 4, pp. 2503-2518

Dragowski, A., Kaczynski, R. and Wroblewski, J., (1988). September. Engineering-Geological Problems Related to the Reconstruction of the Hatshepsut Temple in Deir ElBahari. In Proceedings of the International Symposium on the Engineering Geology of Ancient Works, Monuments and Historical Sites-Preservation and Protection, IAEG,

Dunn, J. (2014) The Geography and Geology of the Valley of the Kings on the West Bank at Thebes. London.

Dupuis, C., Aubry, M. P., King, C., Knox, R. W. B., Berggren, W. A., Youssef, M., Roche, M. et al. (2011). Genesis and Geometry of Tilted Blocks in the Theban Hills, near Luxor (Upper Egypt). Journal of African Earth Sciences, 61, 245-267.

Einstein H H, Baecher G B (1983). Probabilistic and statistical methods in engineering geology. *Rock Mechanics and Engineering Geology* 16 (1): 39–72.

Examine 2D v.8.0 Program from Rocscience (2D stress analysis for underground excavations software)**. http://www.cesdb.com. Examine 2d.**

Hamada M., Aydan O., Tano H. (2004). A report on environmental and Rock Mechanical Investigations for the Conservation Project in the Royal Tomb of Amenophis III. In Conservation of the Wall Paintings in the Royal Tomb of Amenophis III – First and Second Phases Report. pp. 83-138

Hemeda, S and **Pitlakis, K.** (2010). Serapeum temple and the ancient annex daughter library in Alexandria, Egypt: Geotechnical–geophysical investigations and stability analysis under static and seismic conditions. *Engineering Geology* 113, 33-43.

Hemeda, S. (2019). Geotechnical and geophysical investigation techniques in Ben Ezra Synagogue in Old Cairo area, Egypt. Herit Sci 7, 23 (2019). https://doi.org/10.1186/s40494-019-0265-y

Hemeda, S. (2008). An integrated approach for the pathology assessment and protection of underground monuments in seismic regions. Application on some Greek-Roman monuments in Alexandria, Egypt. Ph. D Thesis, Civil Engineering Department, Aristotle University of Thessaloniki, Greece.

Hemeda, S. (2018). Engineering failure analysis and design of support system for ancient Egyptian monuments in Valley of the Kings, Luxor, Egypt. Geoenviron Disasters 5, 12 (2018). https://doi.org/10.1186/s40677-018-0100-x

Hemeda, S. (2019). 3D finite element coupled analysis model for geotechnical and complex structural problems of historic masonry structures: conservation of Abu Serga church, Cairo, Egypt. Herit Sci 7, 6 (2019). https://doi.org/10.1186/s40494-019-0248-z

Hemeda, S., Pitilakis, K., Bakasis, E. (2010). Three – Dimensional Stability Analysis of the Central Rotunda of the Catacombs of Kom El-Shoqafa, Alexandria, Egypt. 5th international conference in geotechnical earthquake engineering and soil dynamics, May 24-29 2010, San Diego, California, USA.

Hemeda, S., Sonbol, A (2020). Sustainability problems of the Giza pyramids. Herit Sci 8, 8 (2020). https://doi.org/10.1186/s40494-020-0356-9

https://doi.org/10.1016/j.jafrearsci.2011.06.001

KV57 (1997) Theban Mapping Project available at:

http://www.thebanmappingproject.com/ [Accessed on 13th to 15th of April 2020]

Layton, P. (1995) The Tomb of Sons of Ramsses II Discovered? *Minerva* 6/4: 12-15.

Lazar, J. (1995). Geologisch-geotechnische Untersuchungen im Thebanischen Gebirge Teil Nord, Luxor Agypten, Universitat Bern, unpublished M.Sc. Thesis, p.161

Litherland, P. (2013) Landscape and human activity in the valley of the kings: seriation, Geology, Construction techniques and their implications in the XVIIITH Dynasty" Master Thesis, Cambridge University.

McLane, J., Wüst, R.A., Porter, B. and Rutherford, J., (2003). Flash-flood impacts and protection measures in the Valley of the Kings, Luxor, Egypt. APT Bulletin, 34: 37-45.

PLAXIS 3D SOFTWARE. INFO@ PLAXIS.COM

PLAXIS Manual, Finite Element Code for Soil and Rock Analysis. Published and distributed by AA Balkema Publishers, Nederland's Comput. Geotech.32 (5). pp326–339.

Reeves, N; Wilkinson, R. (1966) Complete Valley of the Kings, The (Tombs and Treasures of Egypt's Greatest Pharaohs) Thames and Hudson Ltd.

RocLab 1.0 Software program for determing rock mass strength from Rocscience.

Rutherford, J.B., (1990). Geotechnical causes of ancient tomb damage: Valley of the Kings, Egypt. AA Balkema.

Salamon, M.D.G. and A.H. Munro. (1967). A Study of the strength of coal pillars. Journal of South African Institute of Mining and Metallurgy. Vol 68, No 2. pp. 55-67. September.

Siliotti, A. (1997) Guide to the Valley of the Kings. Barnes & Noble Books.

Strudwick, N. & H. (1999) Thebes in Egypt. British Museum Press, London.

Tawfik, H.A., Zahran, E.K., Abdel-Hameed, A.T. and Maejima, W., (2010). Mineralogy, petrography, and biostratigraphy of the Lower Eocene succession at Gebel El-Qurn, West Luxor, Southern Egypt. Arabian Journal of Geosciences, 4(3-4): 517-534.

Theban Mapping Project (2019). Online resources and published material www.thebanmappingproject.com. Accessed 11th April 2019.

Theban Mapping Project. [Regular reports on the work in KV 5 appear on the Project's website, www.thebanmappingproject.com.]

Verdel, T., (1993). Géotechnique et Monuments historiques: Méthodes de modélisation appliquées à des cas Égyptiens. Doctoral Thesis, Institute National Polytechnique de Lorraine.

Weeks, K. R. (1998) The Lost Tomb". William Morrow and Company, New York.

Weeks, K. R. (2006) KV5: A Preliminary Report on the Excavation of the Tomb of the Sons of Ramesses II in the Valley of the Kings. The American University in Cairo Press.

Weeks, K. R. (1994) The Theban Mapping Project: Report of the 1994 Field Season. Cairo: Theban Mapping Project.

Weeks, K.R. (1995) The Work of the Theban Mapping Project and the Protection of the Valley of the Kings." in Wilkinson, R. (ed.), "Valley of the Sun Kings: New Expeditions in the Tombs of the Pharaohs". University of Arizona Egyptian Expedition, Tucson.

Weeks, K.R. (2000) Atlas of the Valley of the Kings. Publications of the Theban Mapping Project, American University in Cairo Press, Cairo.

Wüst, R. and **J. McLane (2000)** Rock Deterioration in the Royal Tomb of Seti I, Valley of the Kings, Luxor, Egypt. *Engineering Geology* 58: 163-190.

Wüst, R.A. and Schlüchter, C., (2000). The origin of soluble salts in rocks of the Thebes Mountains, Egypt: The damage potential to ancient Egyptian wall art. Journal of Archaeological Science, 27(12): 1161-1172.

Ziegler, M., Colldeweih, R., Wolter, A., Loprieno-Gnirs, A., (2019). Rock mass quality and preliminary analysis of the stability of ancient rock-cut Theban tombs at Sheikh 'Abd el-Qurna, Egypt. Bulletin of Engineering Geology and the Environment, doi: 10.1007/s10064-019-01507-0.

Figures

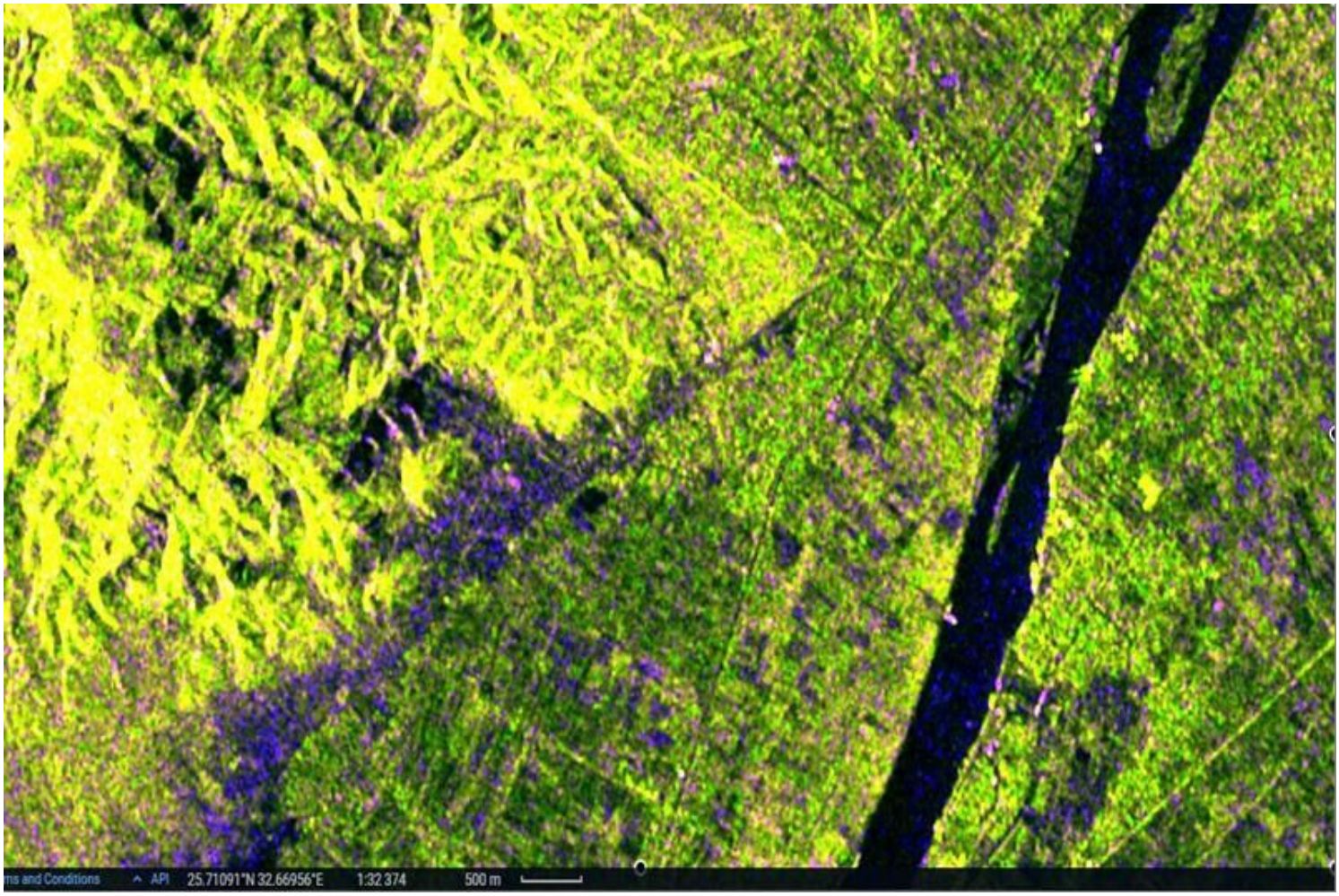

Figure 1

LIDAR image, The Ratio "VV, VH, VV / VH" combination works well for distinguishing water objects, open soils, moistened agricultural fields, vegetation, and urban areas. Water in lakes is shown in dark blue, bright blue or black hues with radar signal noise. Blue hues show agricultural fields with bare soil, often sufficiently waterlogged. Fields with vegetation show a green color. Buildings of a metropolis are represented by bright green-yellow shades.

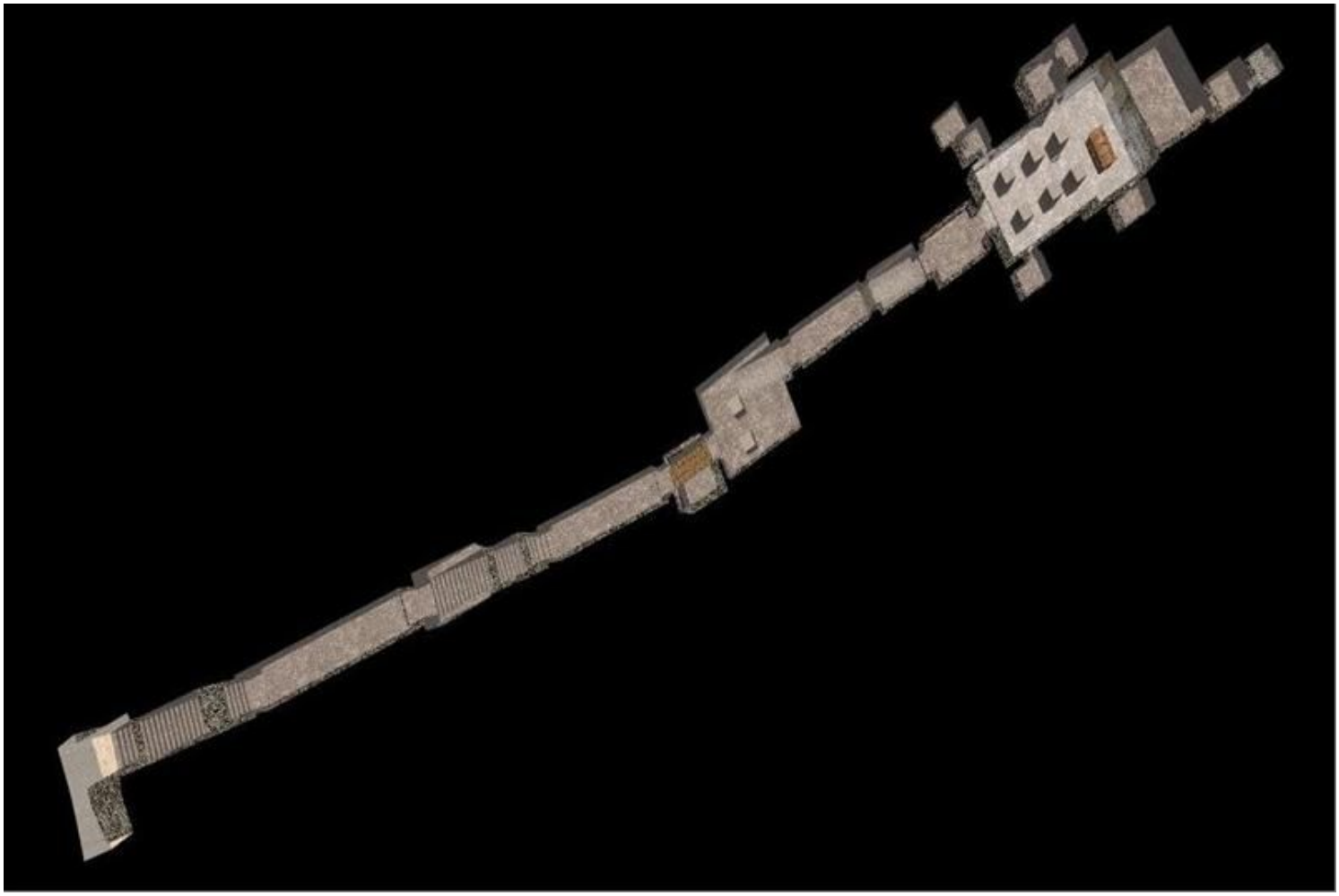

Figure 2

3D Sketchup model for the Horemheb tomb, Luxor, Egypt (KV57).

Figure 3

the entrance and corridor of the KV57 where it is whole excavated in the marl Shale layers, Chert lenses and nodules are abundant and obvious.

Figure 4

In-plane deformation patterns like vertical cracks and crown zone rock falling and intensive cracking of lintel due to over loading (geostatic loading) and impact of old and modern flash floods in particular the 1994 flood.

Figure 5

Extensive structural damage of crown ceiling zones and engineering failure of the structural pillars, sidewalls and Ceiling of the Corridors and Chambers in the KV57. Brittle rock, high stress conditions lead to rockbursting (the sudden release of stored strain energy) bursts manifest themselves through sudden. Extensive rock falls from the ceiling is obvious and cracks are active wher the gypsum Pegs are cracked and broken.

Figure 6

Carved and decorated walls in massive Esna shale Member are in advanced state of disintegration. Showing chert lenses. The ornamented plaster on top of the chert lenses and nodules was damaged during the first flash floods that entered the tomb some 3000 years ago. During several restoration projects over the past 200 years, cracks were filled with plaster for protection and stabilization of the tomb. The impact of the 1994 flash floods on the mural paintings inside the tomb are severely obvious.

Figure 7

Urban Image. This band combination also provides a "natural-like" rendition while also penetrating atmospheric particles, smoke and haze. Vegetation appears in shades of dark and light green during the growing season, urban features are white, gray, cyan or purple, sands, soils and minerals appear in a variety of colors. The almost complete absorption of Mid-IR bands in water provides well defined and highlighted sources of water within the image. water is black or dark blue. Hot surfaces such as forest fires saturate the Mid-IR bands and appear in shades of red or yellow. One particular application for this combination is monitoring fires. Flooded areas should look very dark blue or black.

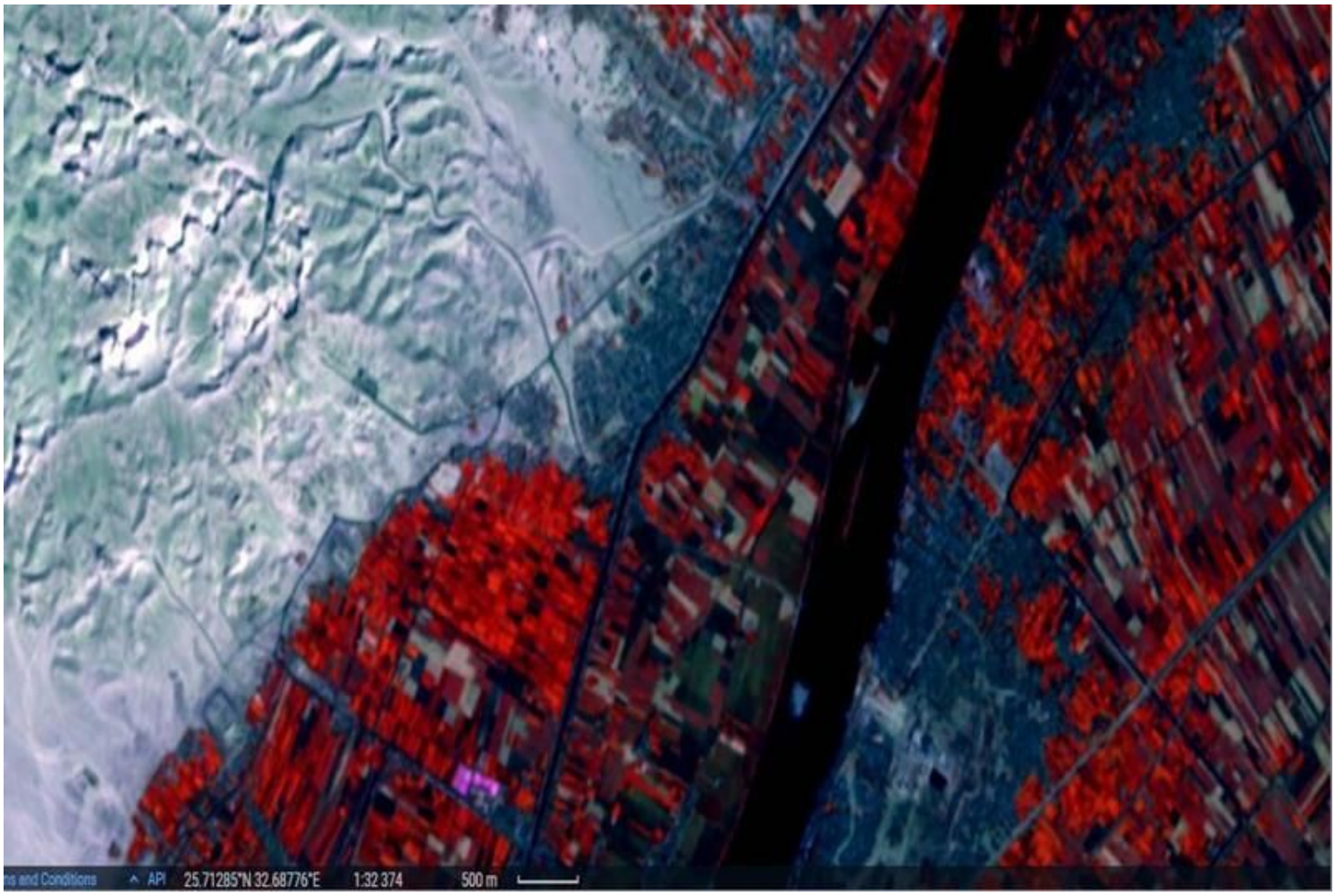

Figure 8

This band combination good for picking out land from water. In this false color image, land appears in shades of orange and green, and water appears in shades of blue.

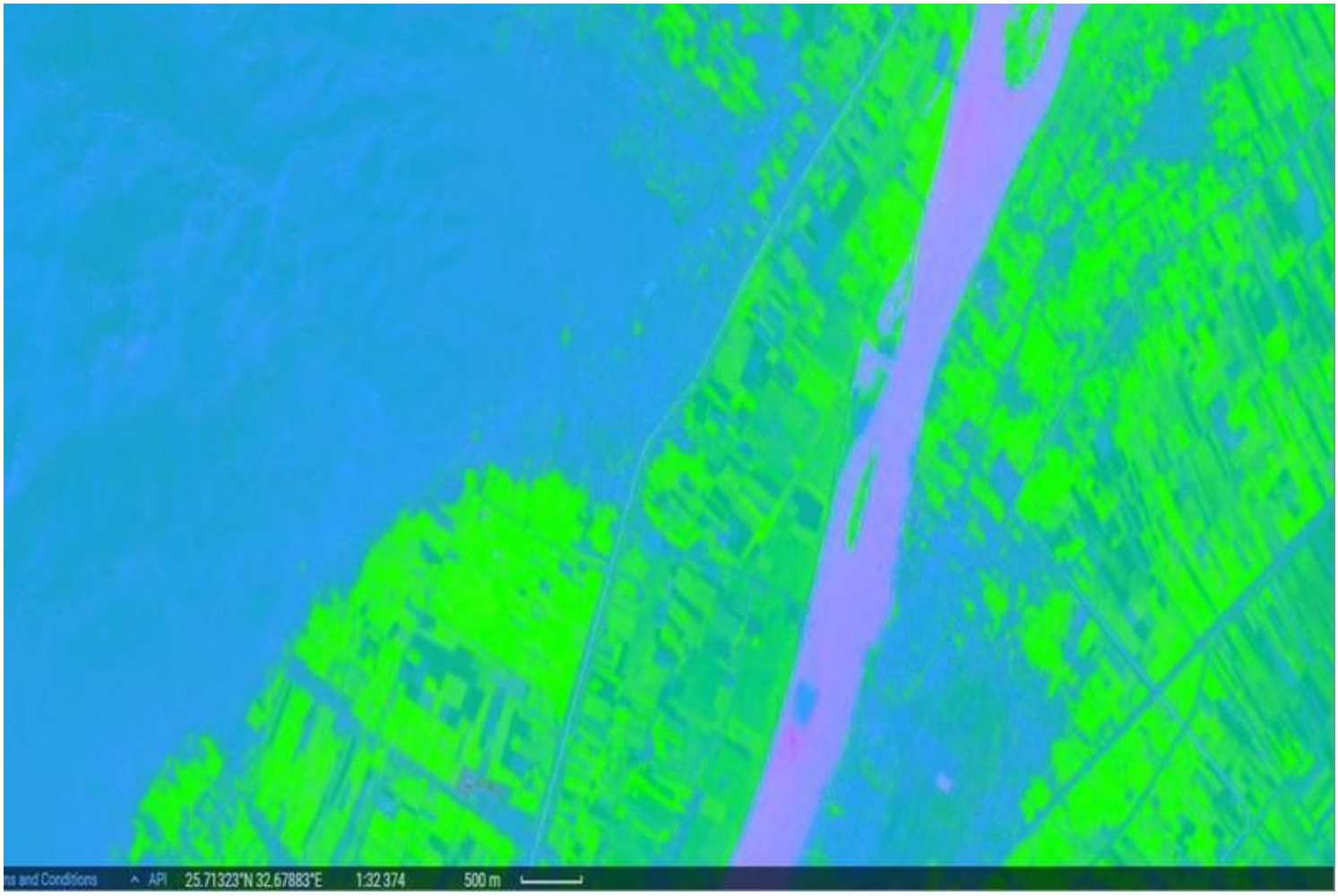

Figure 9

Index stack. It becomes readily apparent in this image stack that particular colors can be equated to different landscape features. For example, vegetation displays here as green, water as purple, and soil, rocks, and barren land as blue. Clouds also appear as a mixture of purple and magenta, so in this case these indices alone are not sufficient for differentiating clouds from water.

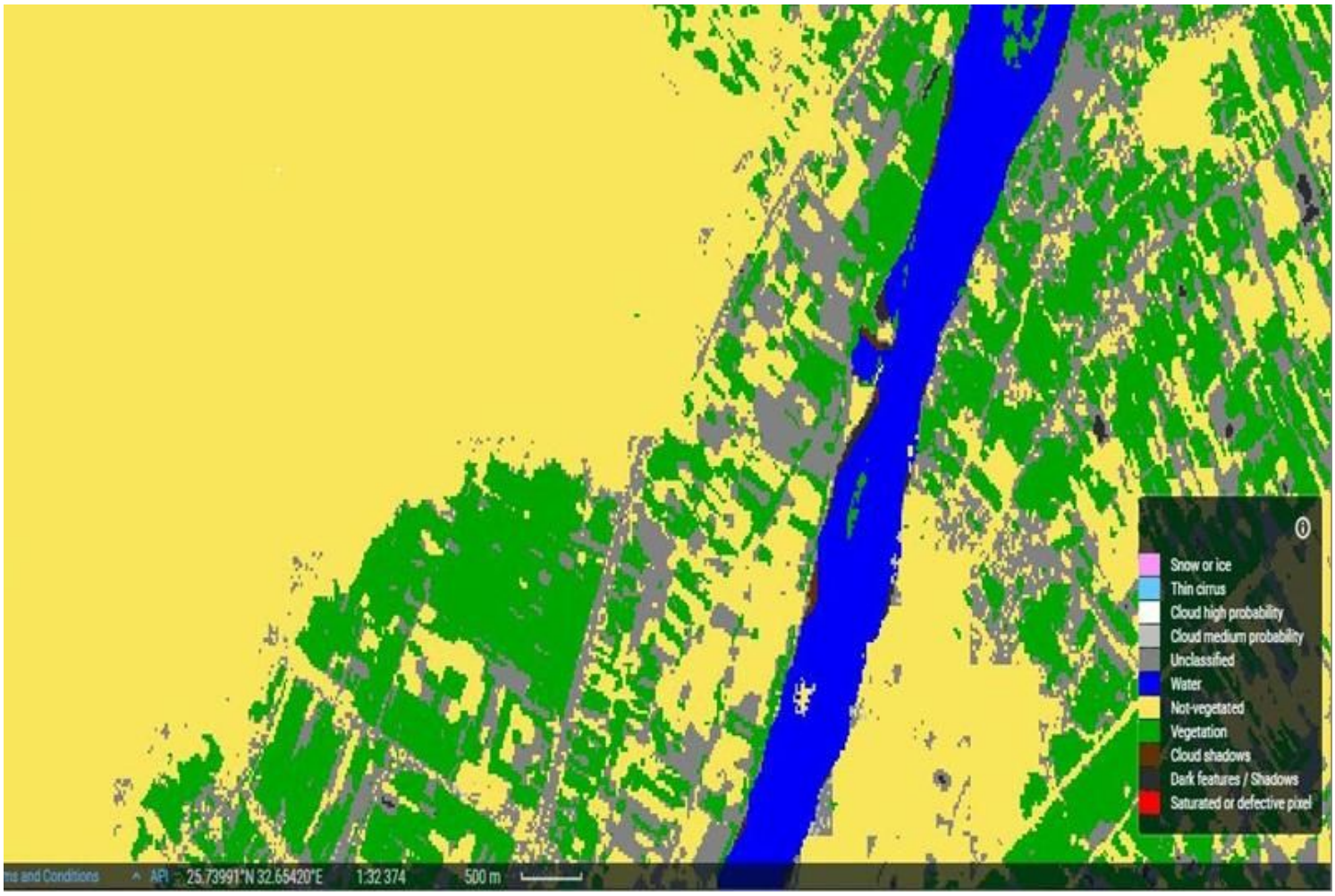

Figure 10

Index stack. It becomes readily apparent in this image stack that particular colors can be equated to different landscape features. For example, vegetation displays here as green, water as purple, and soil, rocks, and barren land as blue. Clouds also appear as a mixture of purple and magenta, so in this case these indices alone are not sufficient for differentiating clouds from water.

Figure 11

Location of the Horemoheb tomb (KV57) at the east (main) Valley of the Kings (KV), Luxor Egypt. Stratigraphical succession as seen. Characteristic weathering of the Thebes Formation was used to subdivide the Thebes Formation into four units, Member I to Member IV. A 30 m displacement of Member I associated to the Kings Valley Fault is located on the right-hand side approximately 40 m from the tomb of Amenmesse (KV10).

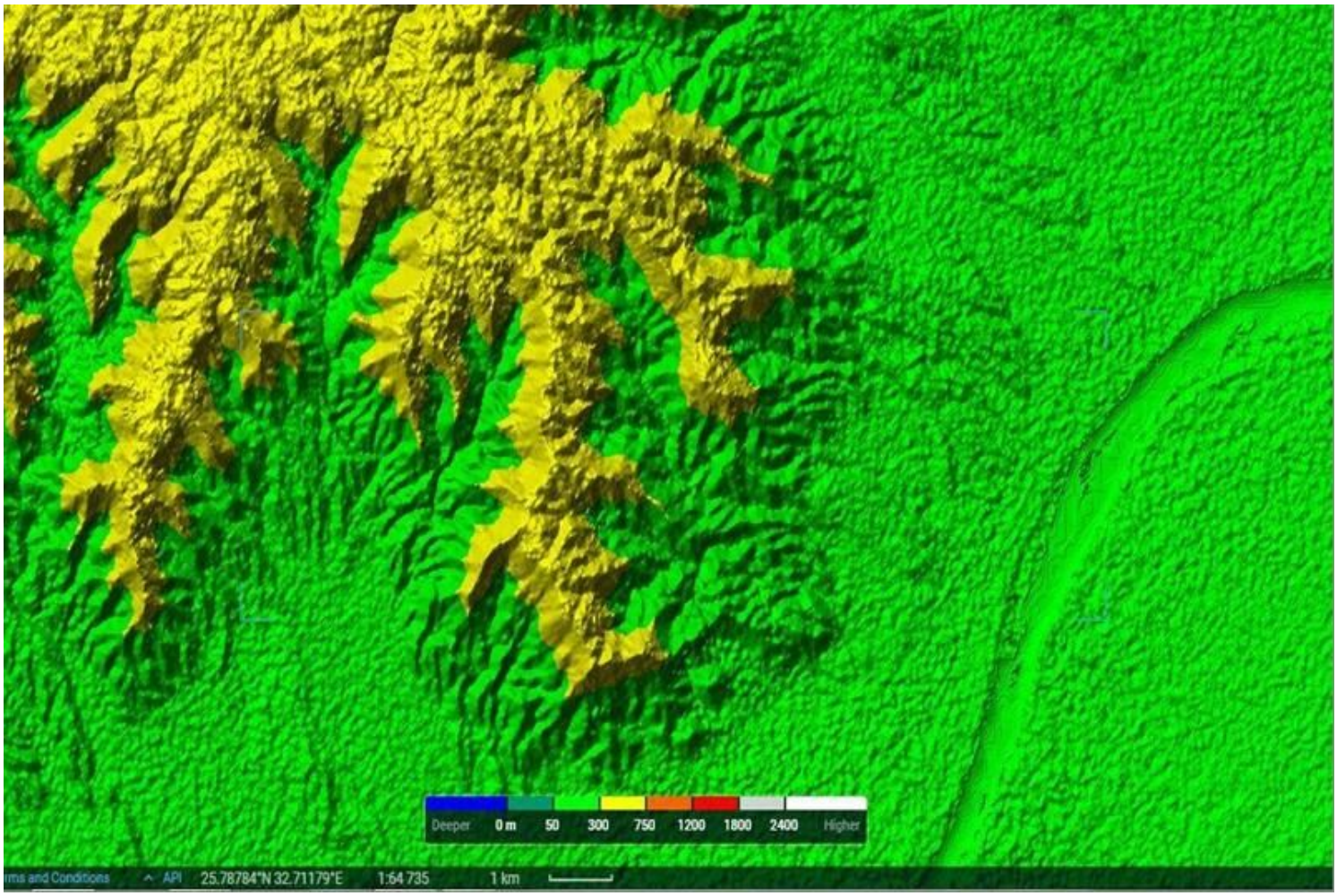

Figure 12

(DEM), Digital Elevation Model of the valley of kings and the Gebel Gurnah.

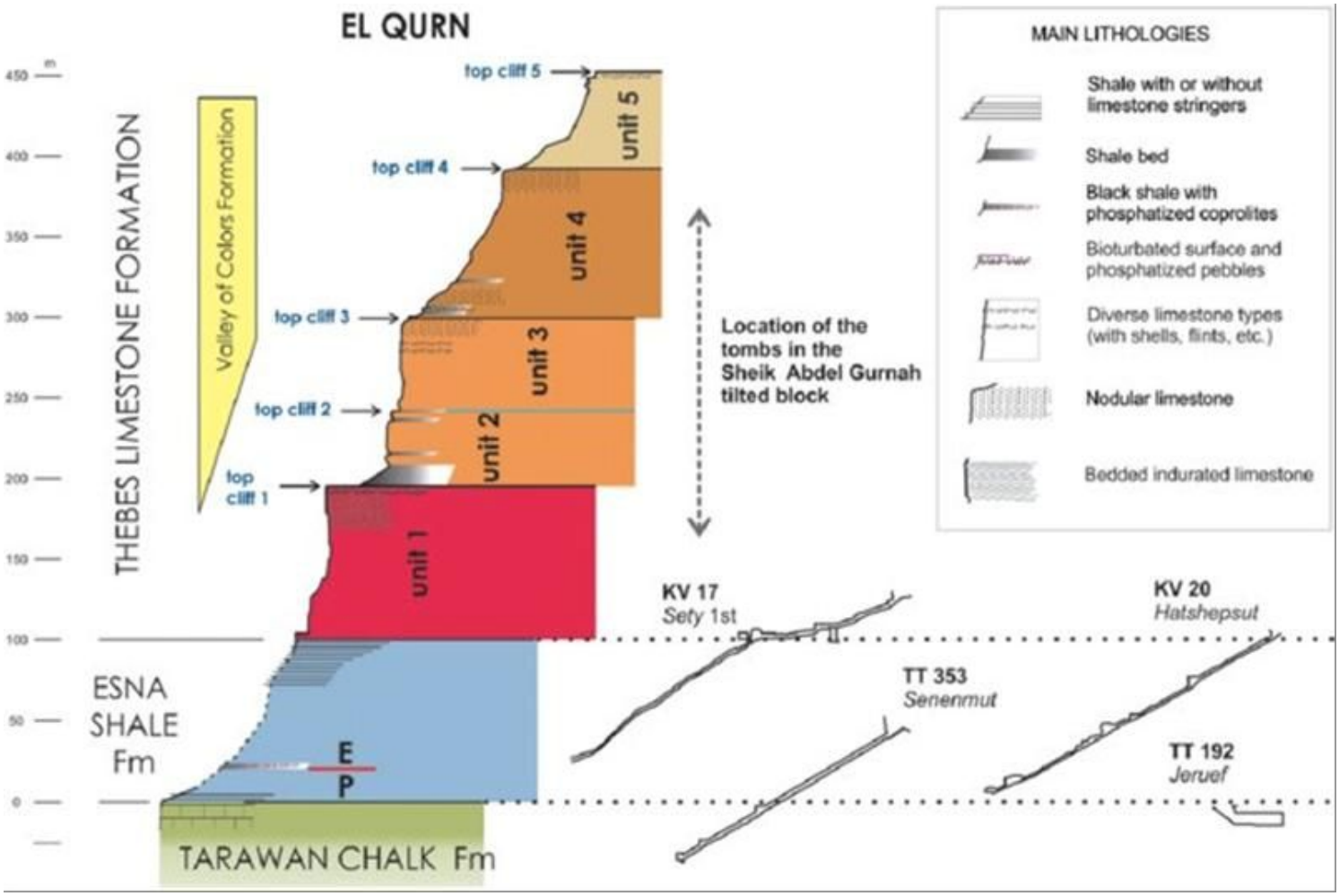

Figure 13

Stratigraphical succession on the West Bank. We show here the location of selected tombs in this succession. Tombs KV17, 20, TT353 and 192 are located in the sub horizontal bedrock. P, Paleocene; E, Eocene.

Figure 14

Abrupt contact of the Abu Had Member of the Esna Shale Formation with lithological unit 1 of the Thebes Limestone Formation. Photo taken just above the location of the KV57

Figure 15

Evidence of flash flood related erosion in the Esna Shale and vertical fissures in Unit 1 of the Thebes Limestone, delineation of the abandoned Excavations and its causeway. The subvertical wall-cuts were dug in the upper part of the Esna Shale Formation and at the base of the Thebes Limestone Formation. White arrows point to erosional gullies in the lower part of unit 1 of the Thebes Formation, in the Hanadi Member (Esna Shale Formation) and in the debris that cover the Esna Formation. Note that the gullies at

the base of the Thebes Limestone and just below are commonly hollowed out, in particular on top and below the prominent base of Unit 1. These are probable evidence of flash floods. fallen blocks; unstable columnar block and open vertical fissures; screes. screes resulting from archeological excavations.

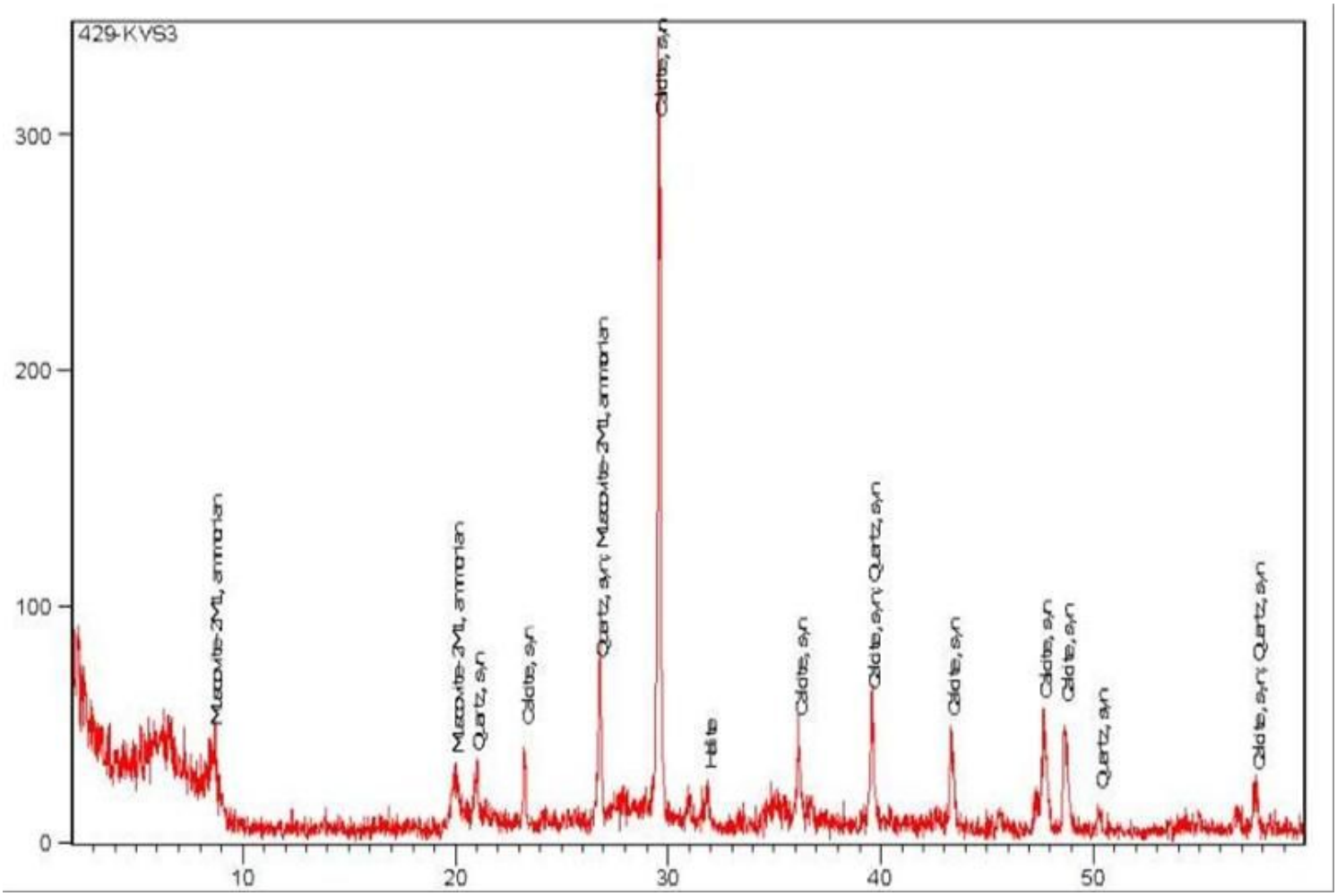

Figure 16

X- ray Diffraction results showing the bulk Mineralogy of Marl Shale (Calcite/ Smectite) where the Horemheb tomb (KV57) is excavated.

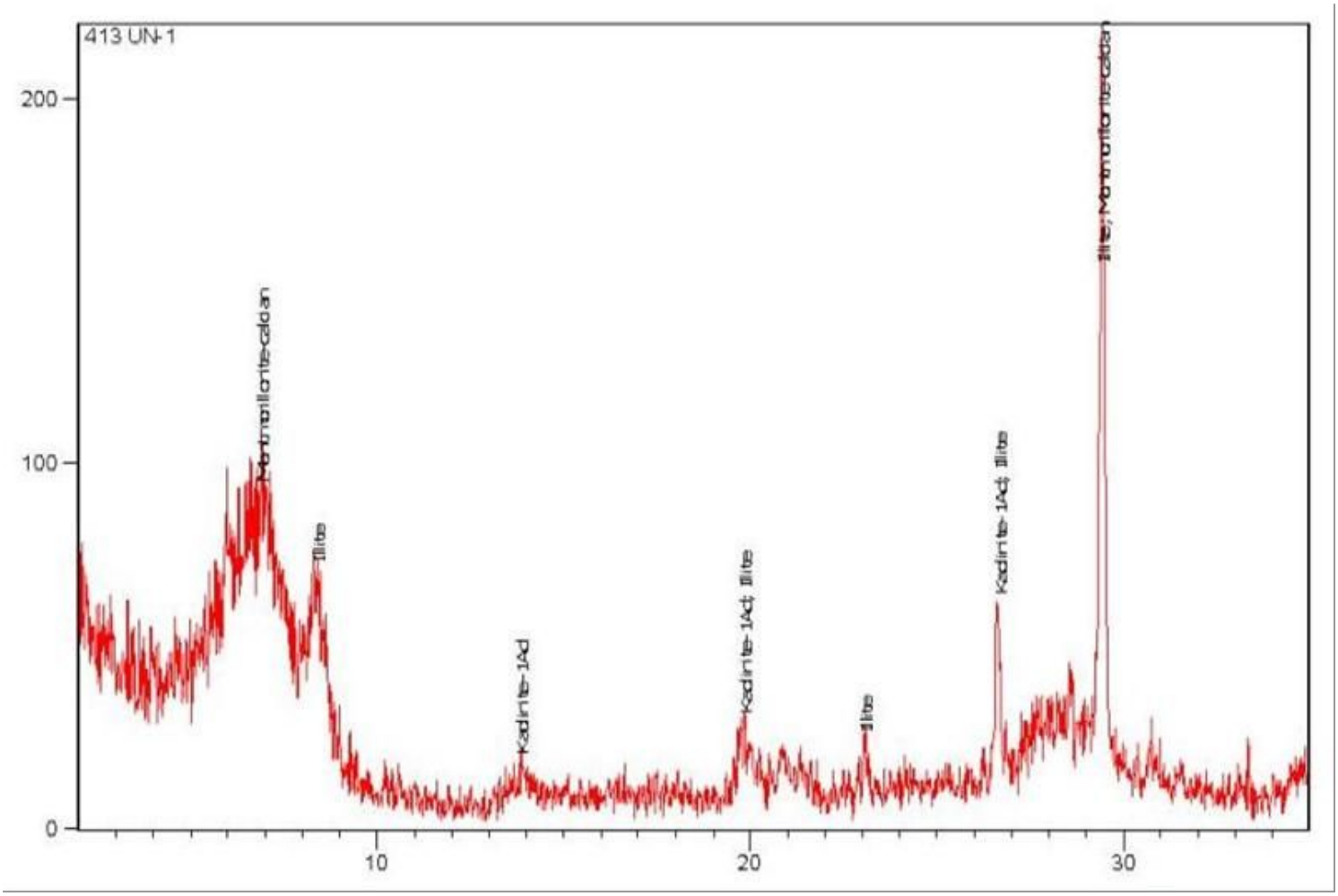

Figure 17

X- ray Diffraction pattern showing the clay minerals of natural or air treated untreated clay fractions sample from Esna shale Member, where the Horemheb tomb (KV57) is excavated.

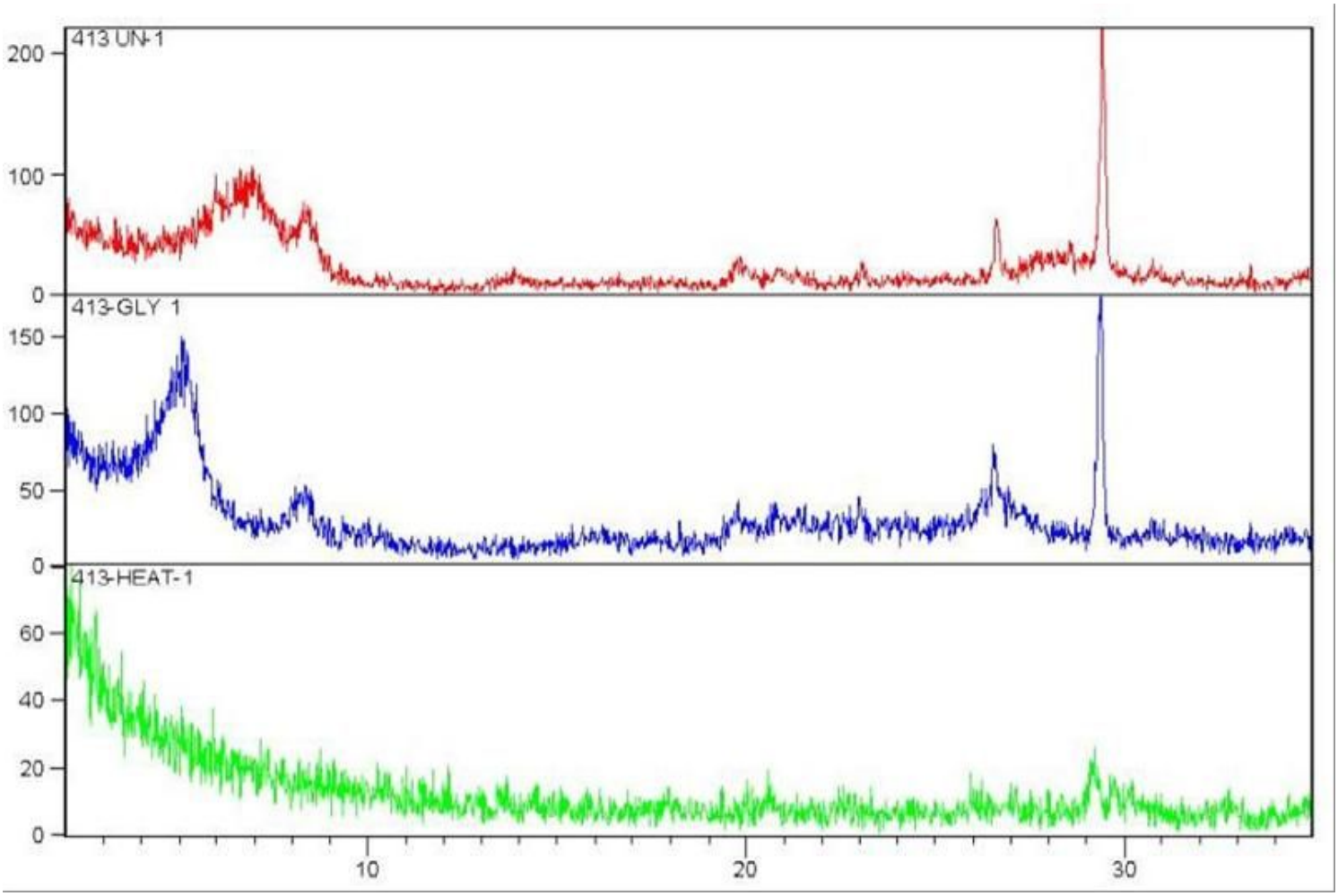

Figure 18

XRD for the air dried, ethylene glycol treated, and heated to 550C clay fractions from samples of Esna shale, showing decrease and disappearance of peak of Illite/Smectite (I/S) and the present of the Montimorillonite.

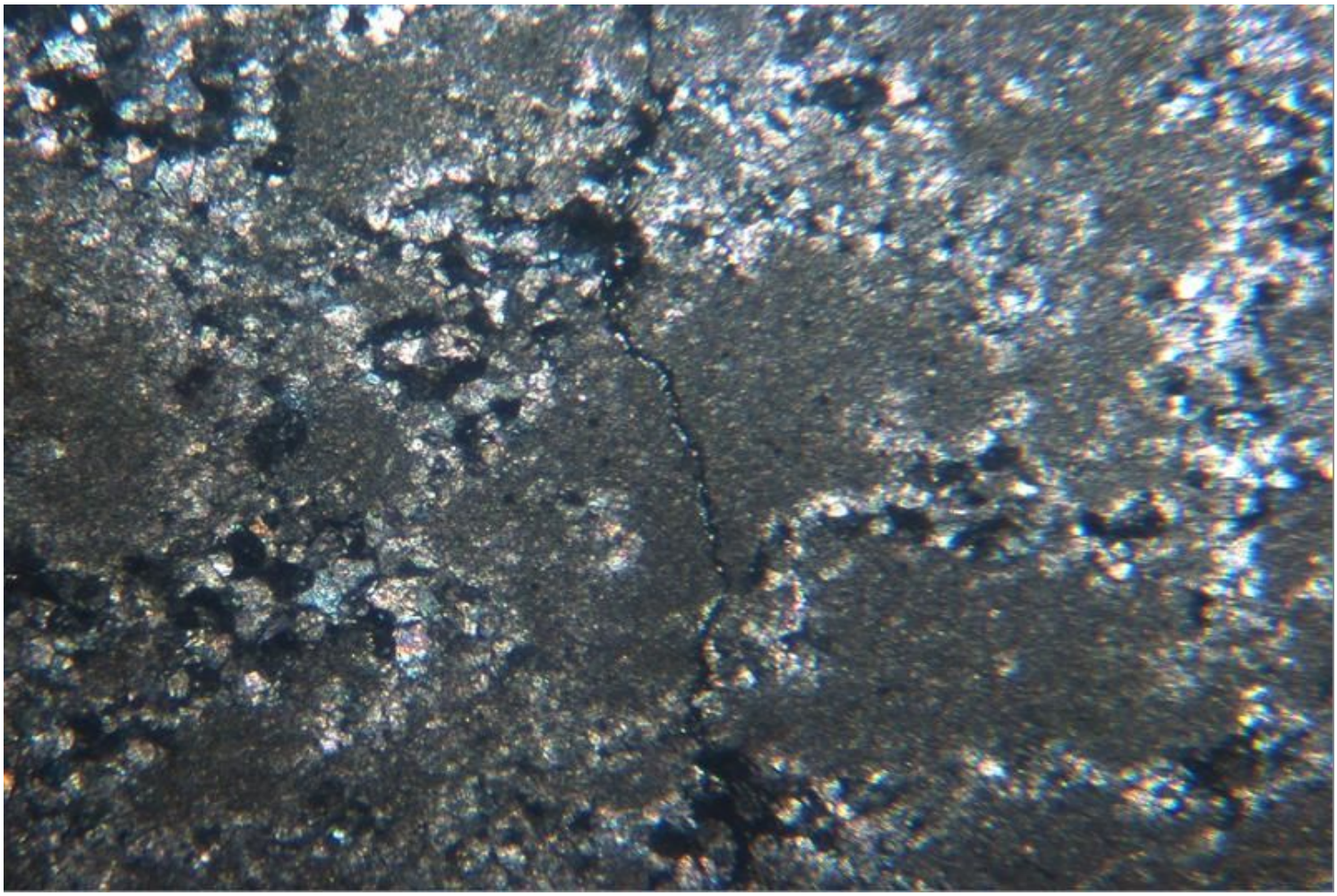

Figure 19

C.N. Microscopic photograph shows The marl sample from Member I is very fine-grained to fine-grained. Considerable amounts of cavities and microvienlets filling by recrystallized dolomite are observed in the micritic calcite matrix. The rock is very to fine-grained and composed mainly of calcite and dolomite as the essential components associated with minor amount of clay minerals and rare amounts of microcrystalline quartz, iron oxides and opaques. Calcite represents the matrix of the rock and occurs as very fine-grained (micrite), anhedral to subhedral interlocked crystals. Dolomite occurs as very fine to fine-grained, euhedral to subhedral crystals and filling microvienlets and cavities. Quartz is detected as very fine-grained crystals scattered in the matrix. Some pores of irregular shapes and various sizes are observed scattered in the rock. Some parts of the sample are stained by iron oxides

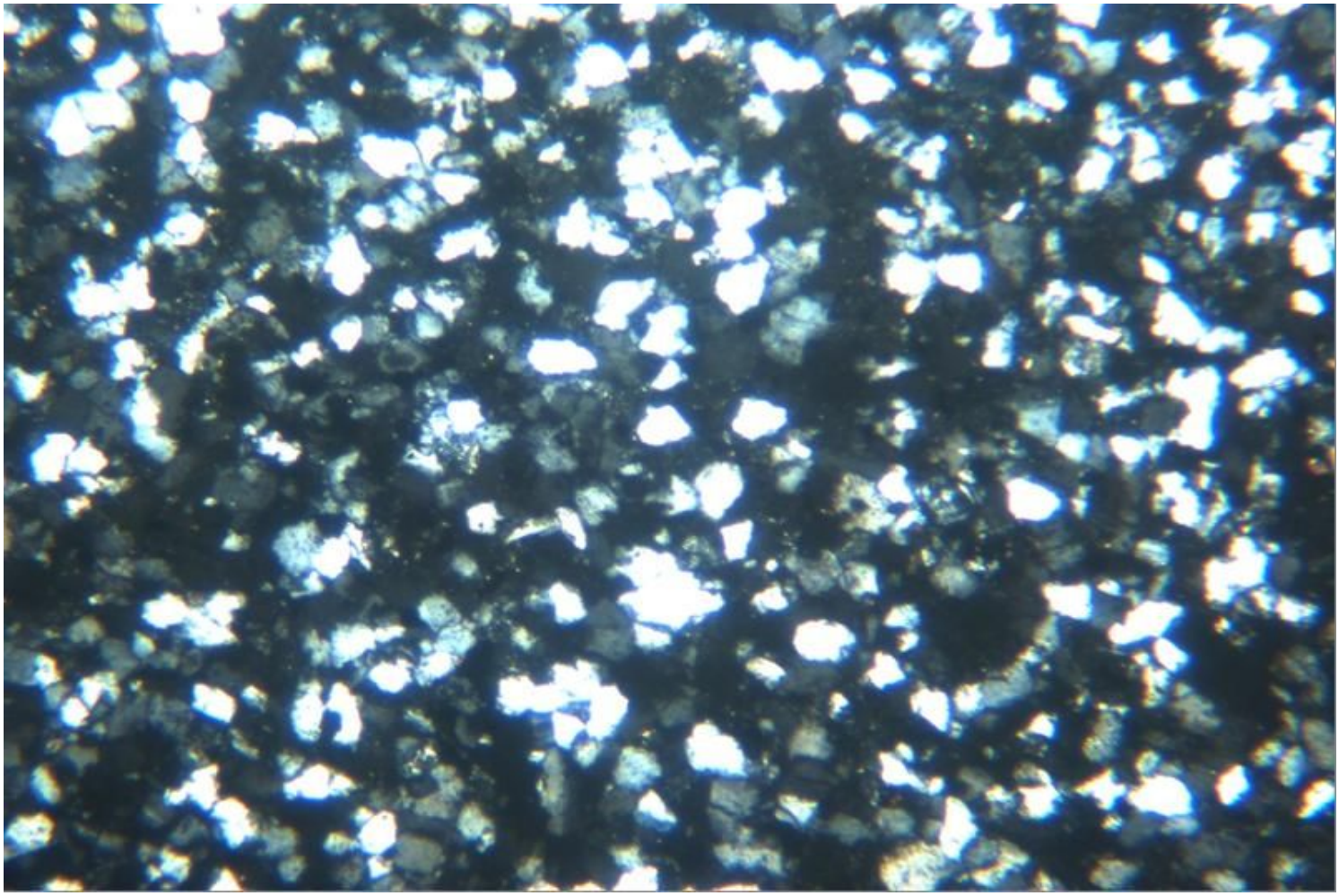

Figure 20

C.N. Microscopic photograph shows the Esna shale sample is very fine to fine-grained (mainly sand size), well sorted that is cemented by minor amounts of iron oxides, clay minerals and carbonates. The sample is porous where pore spaces of different sizes are observed. The rock is composed mainly of quartz and feldspar grains cemented by minor amounts of iron oxides, clay minerals and calcite. Rare amounts of muscovite, biotite, hornblende and opaque minerals are observed in the sample. Quartz occurs as very fine to fine grains of subrounded to angular shape. Feldspars occur as fine grains that are observed in different parts of the sample. Opaque minerals occur as very fine to fine-grained crystals, scattered in the sample. Some parts of the sample are stained by traces of iron oxides

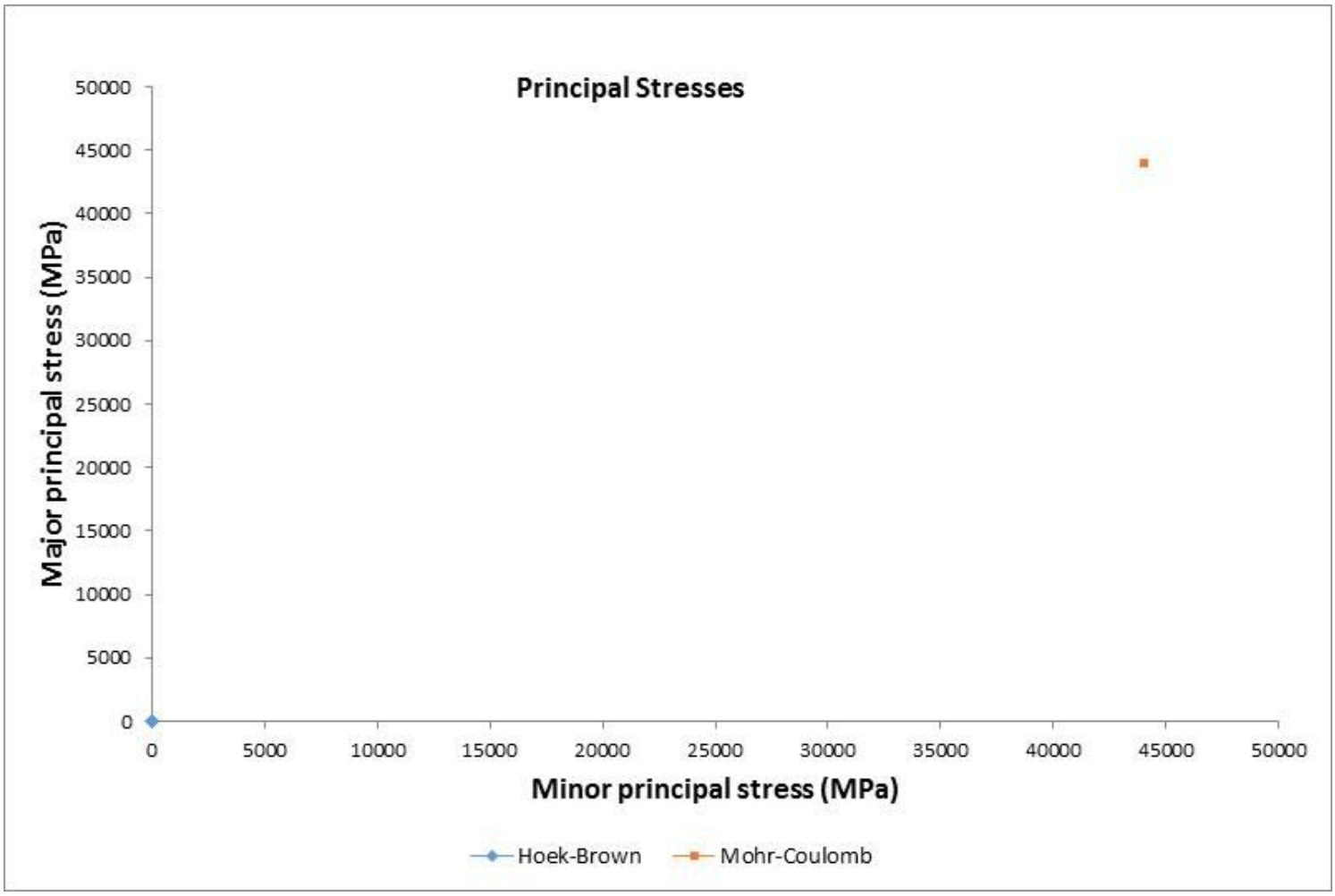

Figure 21

Major and minor principal stress curve of marl limestone (KV57) using the RocLab program.

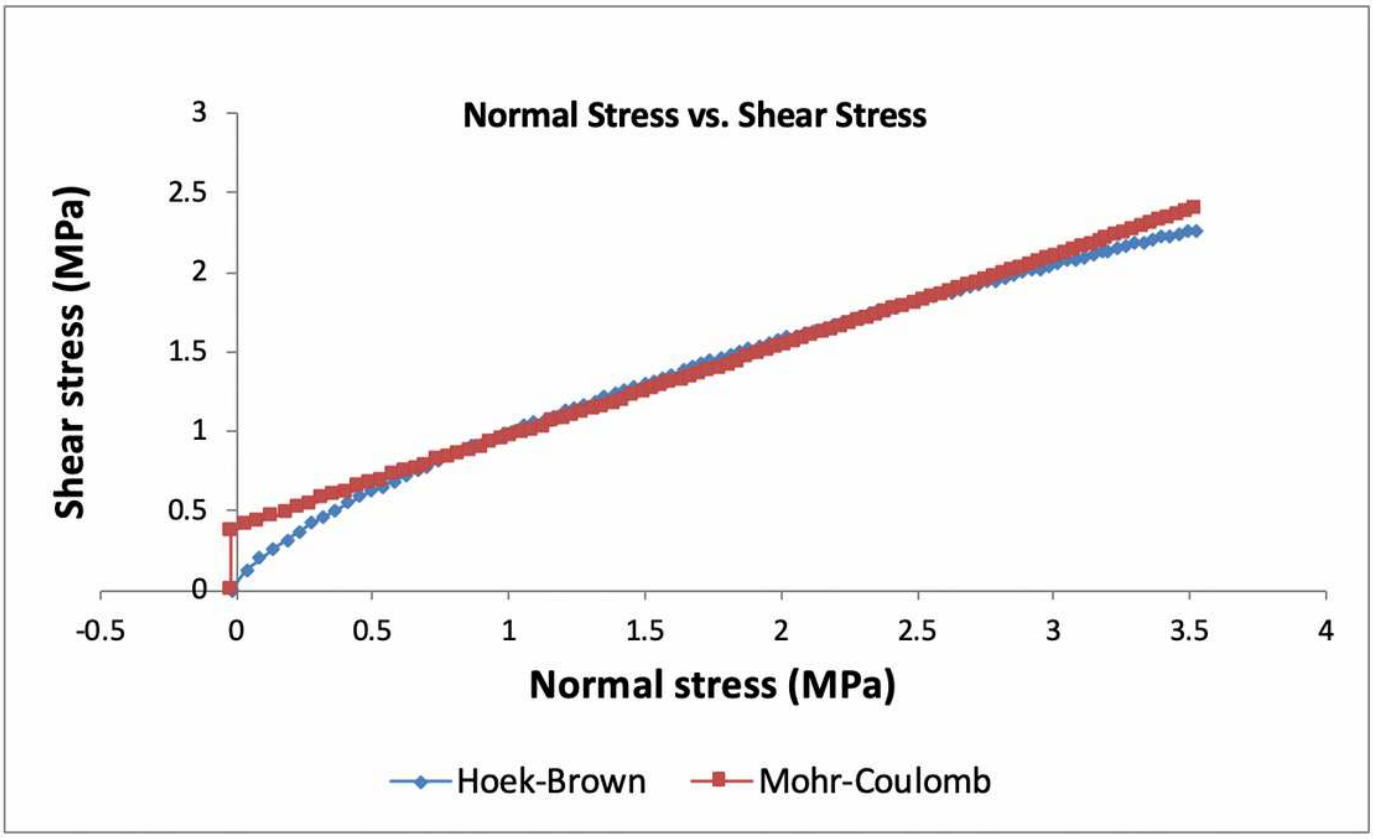

Figure 22

Shear stress-Normal stress curve of Marl limestone (KV57), using the RocLab program.

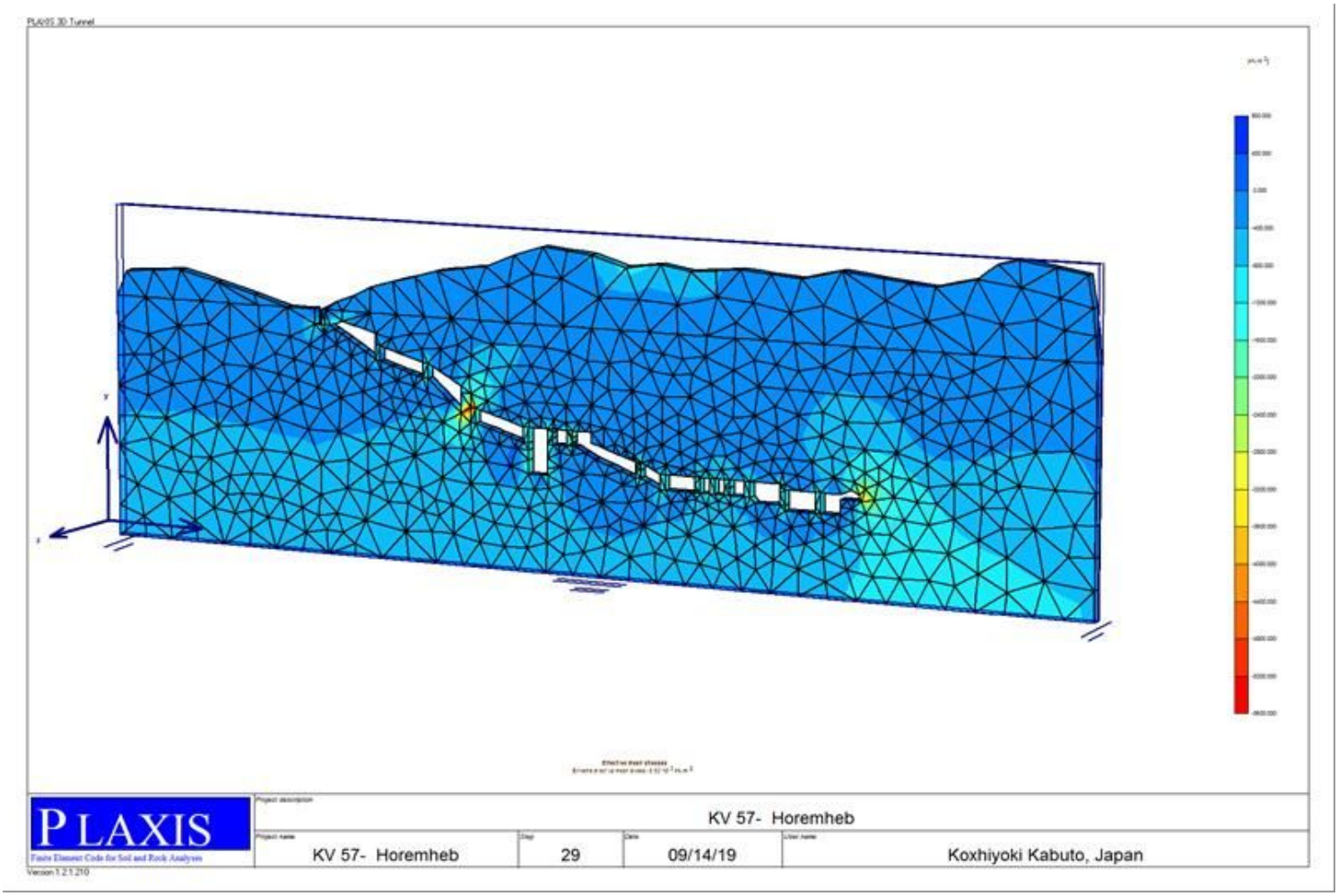

Figure 23

Effective mean stresses for the supported rock pillars and sidewalls in KV57, the extreme value is 5.52*103kN/m2.

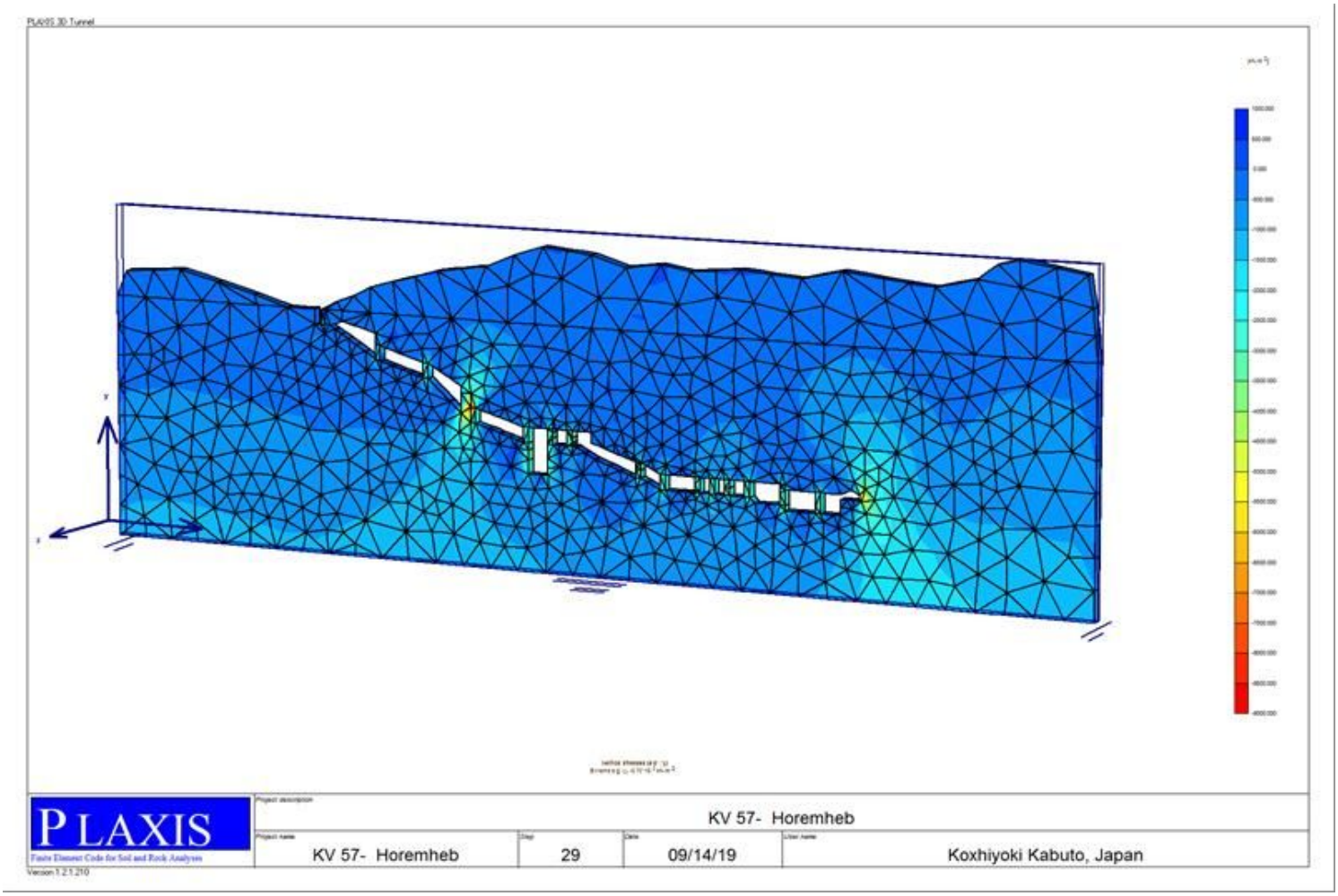

Figure 24

Vertical stresses (sig yy) for the supported rock pillars and sidewalls in KV57, the extreme value is 8.70*103kN/m2.

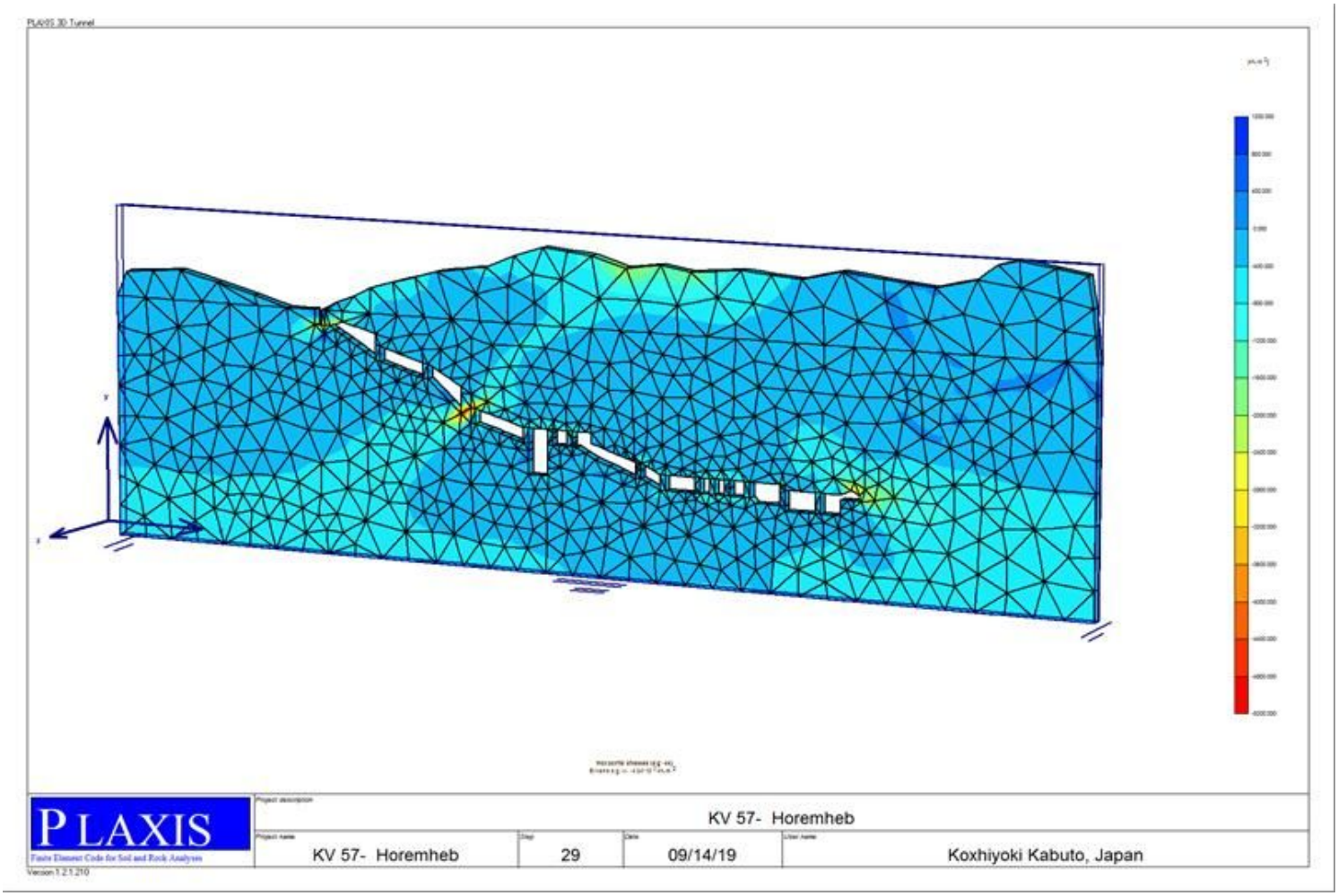

Figure 25

Horizontal stresses (sig xx) for the supported rock pillars and sidewalls in KV57, the extreme value is 4.94*103kN/m2.

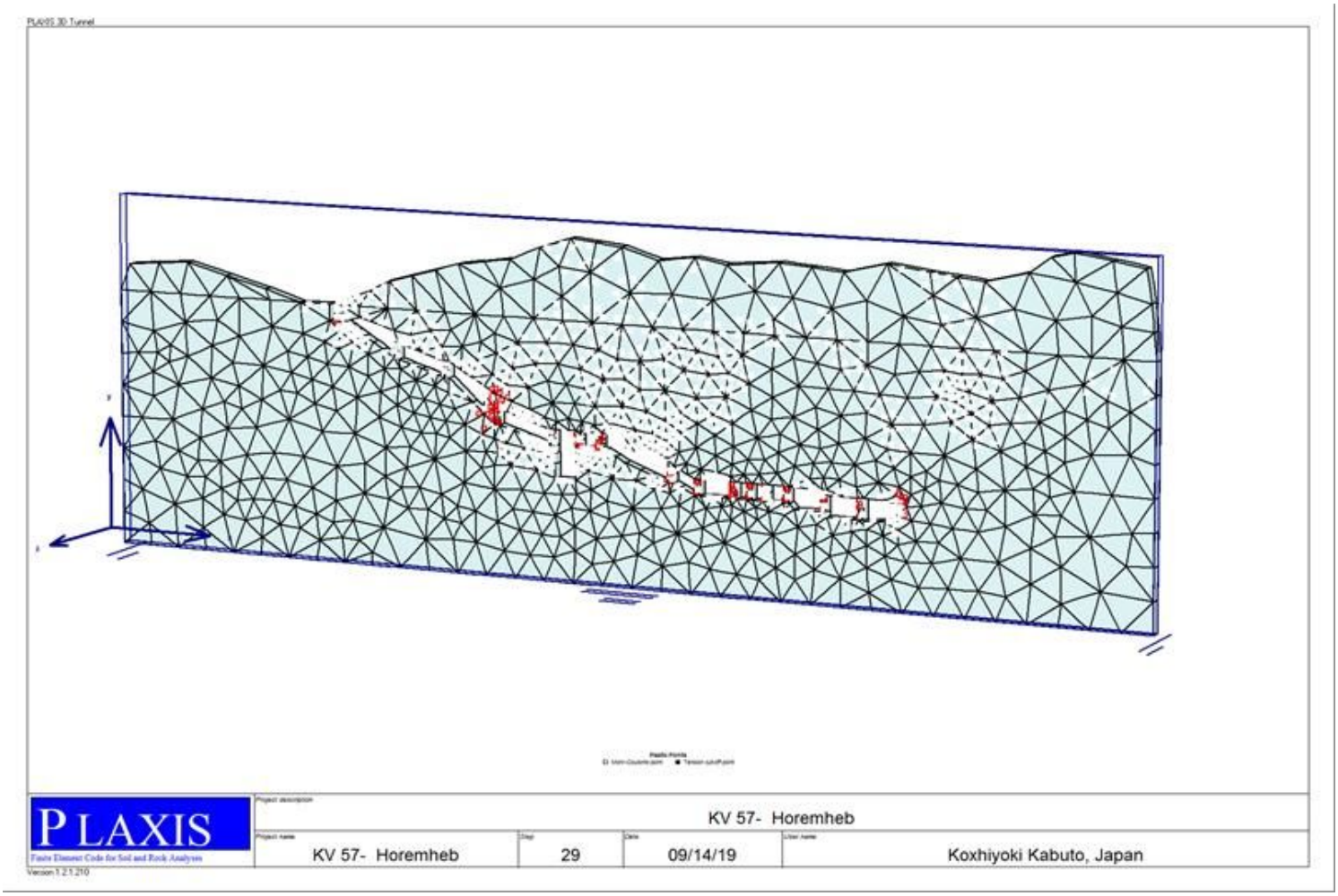

Figure 26

Plastic points (Mohr-Coulomb and Tension cut-off points) for the supported rock pillars and sidewalls in KV57.

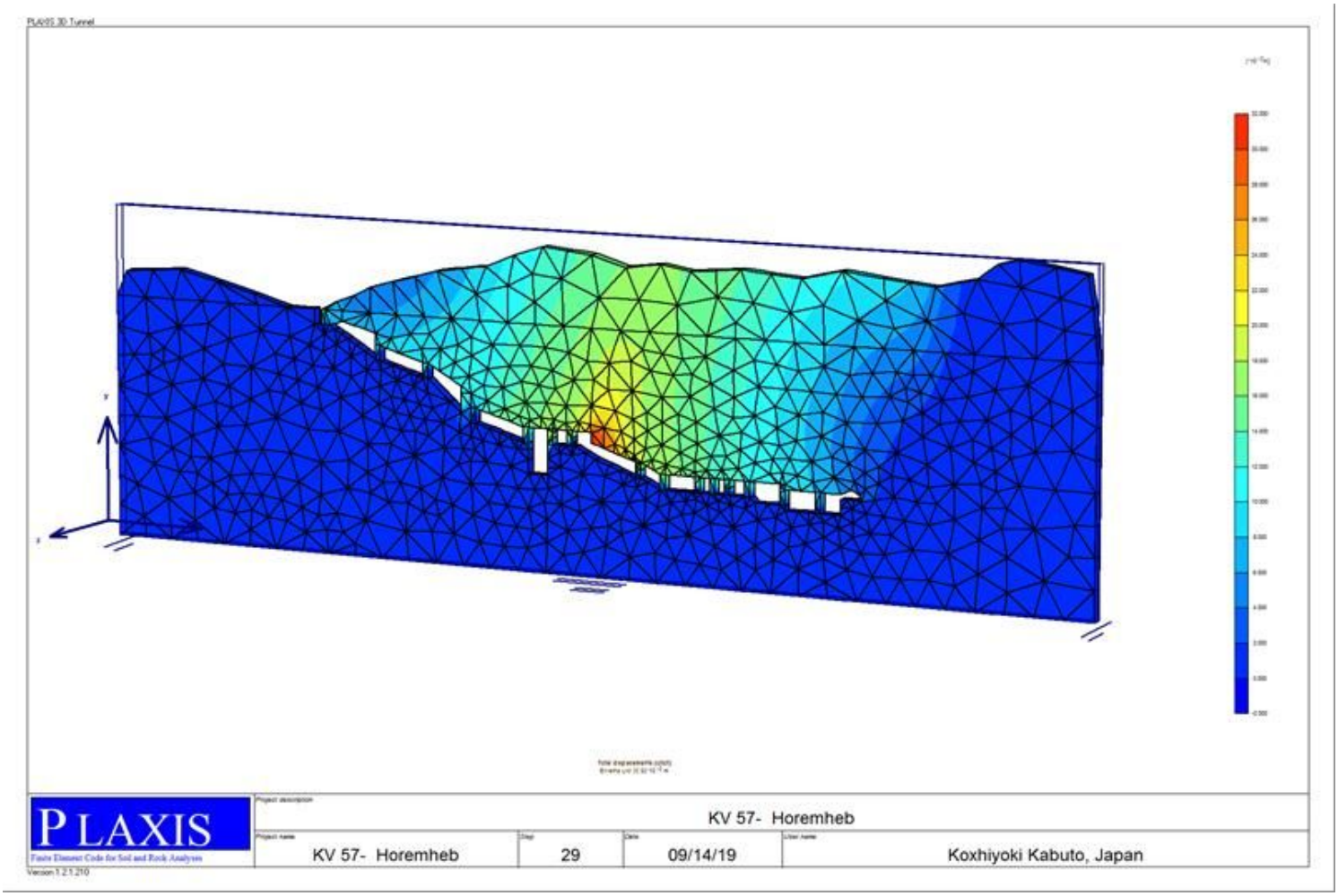

Figure 27

Total displacement (Utot) for the supported rock pillars and sidewalls in KV57, the extreme value is 30.92mm.

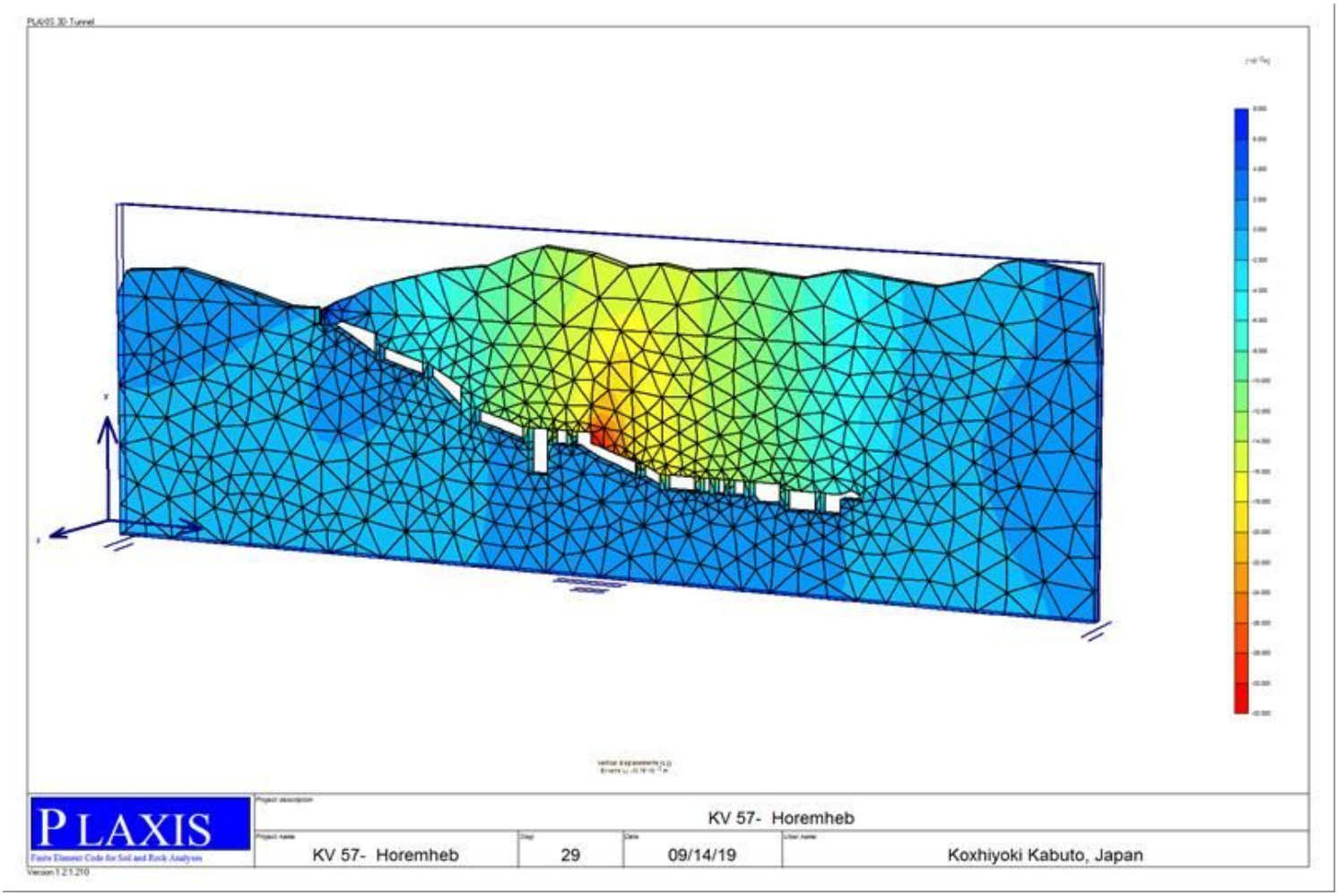

Figure 28

Vertical displacement (Uy) for the supported rock pillars and sidewalls in KV57, the extreme value is 30.76mm.

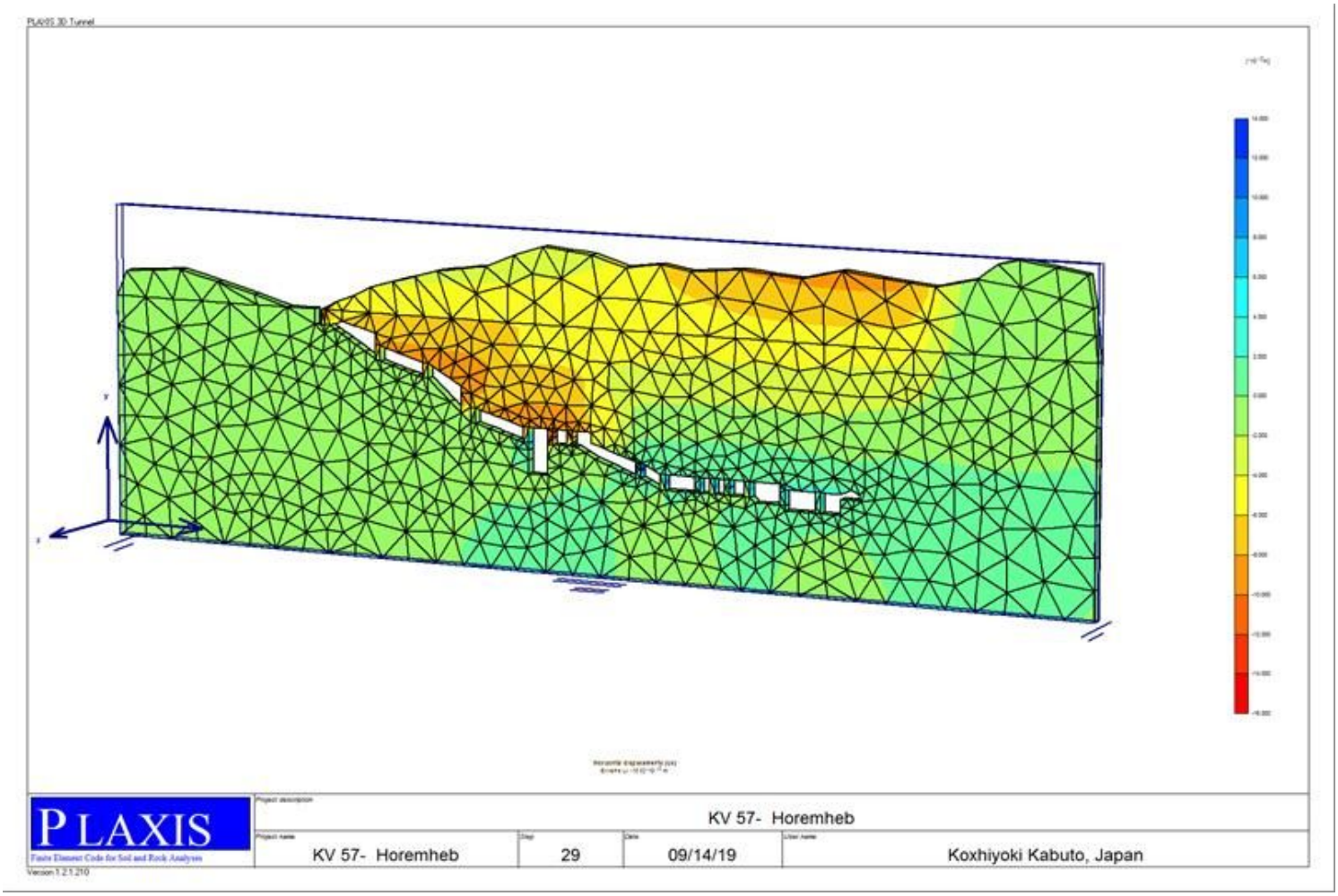

Figure 29

Horizontal displacement (Ux) for the supported rock pillars and sidewalls in KV57, the extreme value is 15.52mm.

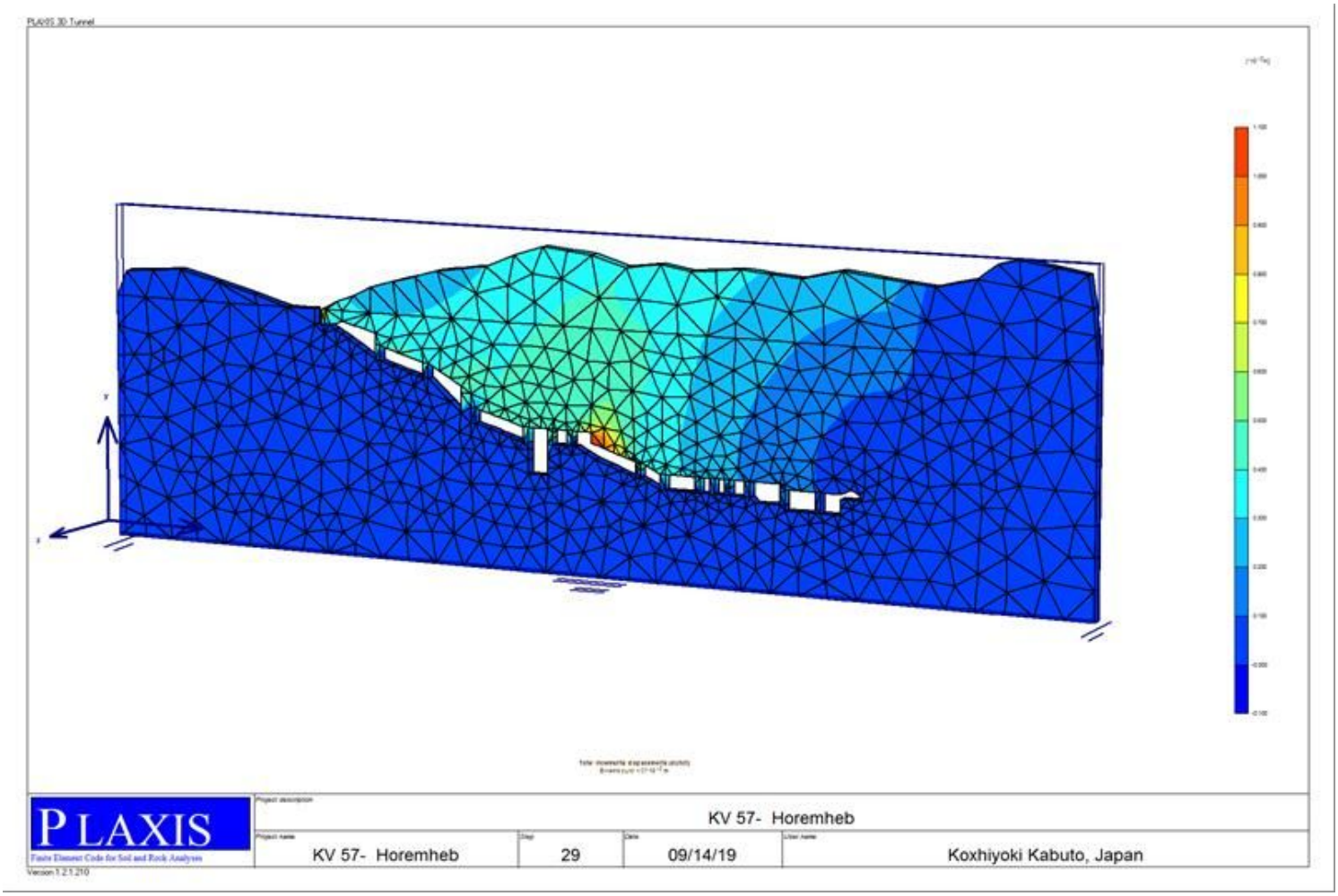

Figure 30

Total incremental displacement (dUtot) for the supported rock pillars and sidewalls in KV57.The extreme value 1.07mm.

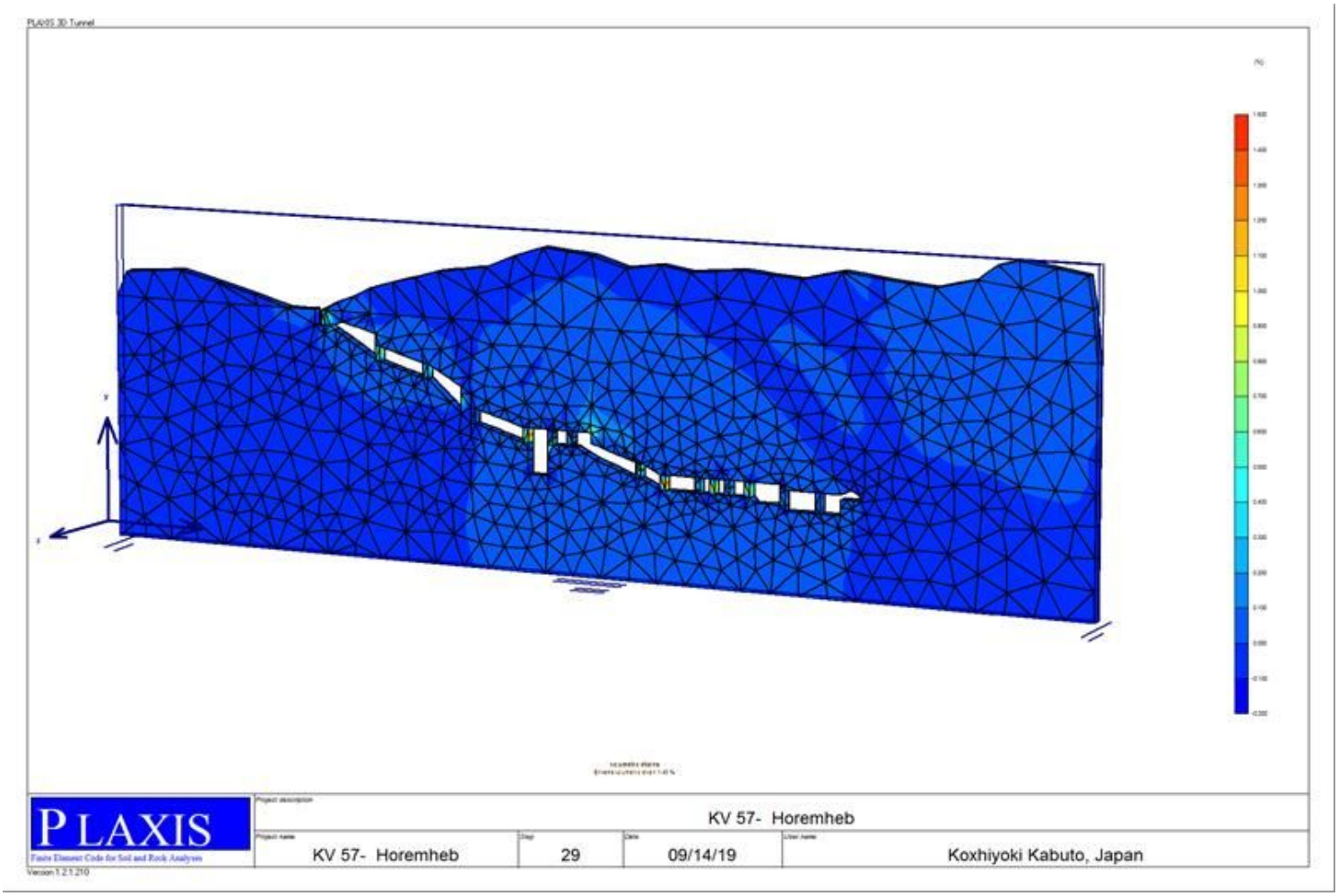

Figure 31

Volumetric strains for the supported rock pillars and sidewalls in KV57.The extreme value 1.45 %.